Photon-echo attenuation by dynamical processes in rare-earth-ion-doped crystals

Felix R. Graf,* Alois Renn, Gert Zumofen, and Urs P. Wild
Physical Chemistry Laboratory, Swiss Federal Institute of Technology, ETH-Zentrum, CH-8092 Zürich, Switzerland
(Received 3 December 1997)

We study the photon-echo attenuation by various dynamical processes in rare-earth-ion-doped crystals. The experimental investigations concentrate on a Pr^{3+}:Eu^{3+}:Nd^{3+} codoped Y_2SiO_5 crystal at low temperatures. Two-pulse photon-echo intensities are measured as a function of the pulse intensities when either the Pr^{3+} or the Eu^{3+} ions are excited. For the quantitative interpretation we consider primarily excitation-induced frequency shifts (EFS) by diagonal and off-diagonal interactions and show that for the systems under consideration EFS are dominated by diagonal interactions. The observed echo attenuation by EFS is compared with the predictions calculated from independent Stark-field measurements and reasonable agreement is obtained. The broadening by spin-ion interactions, by nonequilibrium phonons and the dependence of the echo attenuation on the frequency position in the inhomogeneously broadened band are further investigated.
[S0163-1829(98)09633-7]

I. INTRODUCTION

Solids containing rare-earth (RE) ions have attracted spectroscopists's attention since the beginning of this century.[1] In the last 30 years their extremely narrow spectral features in combination with the use of nonlinear spectroscopy have served to sensitively measure ion-solid interactions.[2] The potential of RE-ion-doped crystals as optical storage materials and processors has lately been a driving force in their investigations.[3] The ratio of inhomogeneous to homogeneous linewidth is regarded as an adequate measure of storage density and can be as large as 10^6 at cryogenic temperatures. Therefore, the analysis of the dynamical behavior and interaction of the host ions with the solid is of fundamental as well as applied interest.

Photon echoes have been extensively employed to study quantum coherence and mechanisms that lead to a destruction of the coherence by dephasing.[4–12] It has become clear that the dephasing depends very sensitively on the dynamics in the environment of the photoactive species, so that photon echoes represent a tool for the investigation of extremely small changes in the environmental conditions. Dephasing is closely related to line broadening, so that investigations of echo attenuation and of line broadening are complementary, yielding similar information on different time scales.[12,13] The analyses of photon echoes in solids have shown that several dynamical processes can give rise to an attenuation of the echoes. Such attenuation has been investigated for photoactive species diluted to low concentrations in crystals of high quality at low temperatures. These investigations have been essential for the understanding of the different attenuation mechanisms and as a result the narrowest spectral lines yet observed in solids have been recorded in RE-ion doped crystals.[14]

The two-pulse photon echoes (2PPE) are calculated from the macroscopic polarization **P** which for delta excitation pulses and for a thin sample can be written as[15]

$$\mathbf{P}=\left\langle \mathbf{P_0}\,\exp\left[i\int_0^{t_{12}}\omega(t')dt'-i\int_{t_{12}}^{2t_{12}}\omega(t')dt'\right]\right\rangle, \quad (1)$$

where the two laser pulses are applied at times 0 and t_{12} and the echo is expected to take place at $2t_{12}$. The polarization $\mathbf{P_0}$ depends on the Rabi frequency, the pulse durations, the width of the inhomogeneously broadened band, and on the density of the photoactive species. For simplicity we disregard the vectorial property of the polarization. $\omega(t)$ in Eq. (1) is the transition frequency of the guest ion that changes from ion to ion and fluctuates in time. When averaging is performed, these fluctuations lead to a dephasing and thus to an attenuation in the echo intensity I, which is calculated from $I\sim|P|^2$. The average in Eq. (1) has to be taken over the temporal realizations of $\omega(t)$, over the spectral density of the ion transition, and over the spatial realizations of the environmental configurations of the RE ions.

Several dynamical processes have to be considered in the analyses of photon-echo attenuation. Naturally, these processes simultaneously affect the excitation coherence so that it is not easy to unscramble the various terms contributing to the echo attenuation. To discuss the different attenuation effects we consider the following scheme:

$$\Gamma=\Gamma_{\mathrm{LT}}+\Gamma_{\mathrm{EQP}}+\Gamma_{\mathrm{TLS}}+\Gamma_{\mathrm{SI}}+\Gamma_{\mathrm{EFS}}+\Gamma_{\mathrm{NQP}}. \quad (2)$$

We point out that the individual broadening mechanisms do not necessarily lead to an exponential attenuation of the echo intensity so that expression (2) is only a schematic representation of the broadening. In Eq. (2) Γ_{LT} represents the lifetime limited value, Γ_{EQP} stands for contributions from equilibrium phonons, and Γ_{TLS} takes into account effects due to lattice two-level systems (TLS). Γ_{SI} results from the spin-ion interaction (SI) between the nuclear spins of the RE and the host ions. Γ_{EFS} describes effects arising from interactions between the guest ions. This effect is usually termed as instantaneous diffusion or excitation induced frequency shifts (EFS); in what follows we will use the latter one. Finally, Γ_{NQP} takes into account the broadening by nonequilibrium phonons (NQP). These different broadening mechanisms have been studied over the last three decades. We discuss them independently in this paper and begin with an overview.

The first term in Eq. (2), Γ_{LT}, covers contributions from radiative and nonradiative decays and establishes the ultimate limit of Γ. It can be evaluated in different ways, one being the measurement of fluorescence decays. At cryogenic temperatures, the lifetime of RE ions in crystals ranges from μs up to ms. The reason for such long lifetimes lies in the electronic structure of the ions with partially filled $4f$ electron shells that are well shielded by outer shells from the perturbing crystal field. An overview of RE-ion spectroscopy data is given in Ref. 2.

Γ_{EQP} addresses the broadening by phonons at thermal equilibrium;[16,17] one- and two-phonon processes have been taken into account. Γ_{TLS}, referring to lattice two-level systems, is a weak effect in RE-ion-doped crystals and has only rarely been the subject in the analyses of these systems. However, for crystals grown under different conditions, Flinn *et al.*[18] observed a tremendous change of the extrapolated zero-intensity broadening and a change of the temperature dependence from a T^7 law to a linear behavior. The latter behavior is known for glassy systems[19] and has been interpreted in terms of the standard TLS model.[20,9]

Γ_{SI} depends on the dynamics of the host spins that magnetically interact with the guest ions. This type of phenomenon was studied by Anderson and Weiss[21] to describe the line shapes observed in paramagnetic resonance. Klauder and Anderson[15] initiated the notion of the aforementioned sudden-jump model that was studied in detail and was extended to the standard TLS model.[22–26] Optical evidence for spin-ion interactions was given first by Shelby and Macfarlane[27] in Pr^{3+}:LaF_3 and was confirmed by Monte Carlo simulations.[28] Weak permanent magnetic fields of the order of 100 G were applied to slow down the spin dynamics, which allowed the measurement of linewidths very close to the lifetime limit.[14,29] A particular case arises when the guest ion has a large enhanced magnetic-dipole moment in the excited state. In such a case, the lattice spin dynamics is not uniform in the crystal, rather the dynamics of the lattice spins is frozen-in close to the guest ions. This effect has been discussed in terms of the ''frozen-core'' model.[30] Consequently, the echo decay is modified and can be described by $\ln(I/I_0)\sim-(4t_{12}/T_M)^x$ for short t_{12} where $x=2$ denotes the regular case and $x>2$ indicates a frozen-core effect.[30]

The four first terms in Eq. (2) depend on the properties of the guest-host system and do not depend on the number of excited ions involved in the echo formation. This is different for Γ_{EFS} and Γ_{NQP}. Excitation-induced frequency shifts (EFS) in the optical regime have been proposed by Taylor and Hessler[24] for the interpretation of the concentration-dependent dephasing reported by Liao and Hartmann.[31] Unambiguous experimental evidence of EFS in RE-ion-doped crystals was first given by Cone and Liu[8] and Huang *et al.*[5] Further experimental[10,11,32–34] and theoretical studies[35–37] have been devoted to EFS. The theoretical models were initially based on off-diagonal ion-ion interactions.[38,39,35] It turned out that the averaging over the temporal realizations of the excitation dynamics and over spatial and energetic configurations is involved. Asadullin[37] applied a mean-field type of approach for the analysis of dephasing by EFS. Macfarlane and Shelby[4] observed a broadening in 2PPE depending on the frequency position in the inhomogeneous band and explained their observations in terms of off-diagonal or quasiresonant interactions. These findings were analyzed in more detail by Root and Skinner[36] in terms of off-diagonal interactions. Later it was speculated that diagonal interactions may dominate in EFS.[29] Huang *et al.*,[5] Mitsunaga *et al.*,[10] and Altner *et al.*[40] applied a separate laser to independently induce a high excitation density and the 2PPE intensities were recorded as a function of this density. These experiments made clear that diagonal interactions can lead to a strong attenuation. However, it remained unclear whether diagonal or off-diagonal interactions dominate in pure 2PPE experiments.

Finally, the last term in Eq. (2), Γ_{NQP}, accounts for nonequilibrium phonons[41] (NQP) that are generated by the decay of the electronic excitations. In a bichromatic experiment, Macfarlane and Meltzer[7] pumped an upper Stark level. An increased line broadening was observed that was interpreted in terms of NQP generated by the phonon-assisted relaxation of the upper into the lower level. Kröll *et al.* observed a dephasing in a standard 2PPE experiment, which could not be explained in terms of EFS and the authors conjectured a broadening by NQP.[42,43] By a variation of the focal area, Bai and Kachru[6] clearly demonstrated that NQP play an important role in the dephasing for Pr^{3+}:$YAlO_3$.

In the present work we report on the investigation of 2PPE in a codoped Eu^{3+}:Pr^{3+}:Nd^{3+}:Y_2SiO_5 crystal. For the interpretation we distinguish between different broadening effects. Particularly we concentrate on the EFS broadening by diagonal and off-diagonal interactions. We analyze the characteristic behaviors of the echo decays and compare the order of magnitudes of the two EFS contributions. An experiment is presented that allows one to distinguish between EFS by diagonal and off-diagonal interactions. The absolute magnitude of the broadening by EFS is calculated and compared with the experimental data. Finally, possible broadening contributions of nonequilibrium phonons are estimated

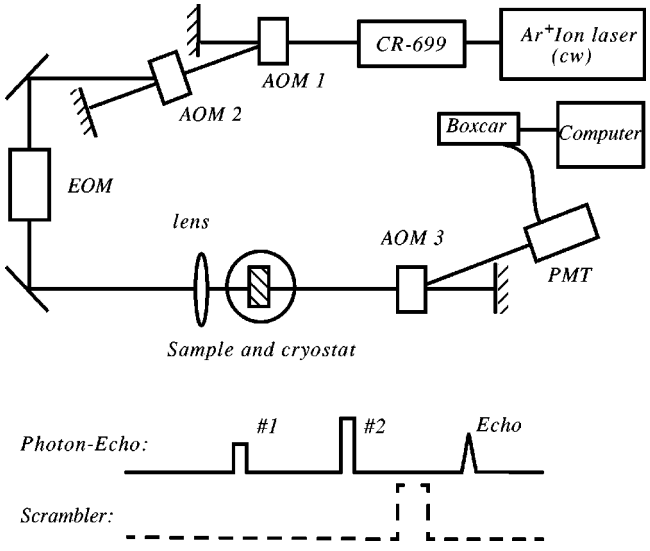

FIG. 1. Experimental setup. The light from an argon-ion-pumped Cr 699 dye laser was chopped by two consecutive AOM. For some of the experiments a third pulse was applied (dashed line). The AOM driver allowed for fast rf-frequency switching (50 MHz/50 ns), so that the frequency of a third pulse could be shifted relative to that of the echo excitation pulses. An electro-optical modulator allowed separate control of the pulse amplitudes.

TABLE I. Spectroscopic data of the present work and taken from the literature for Pr^{3+} and Eu^{3+} in Y_2SiO_5 crystals. The units are given in parentheses. The homogeneous line broadening Γ_h are the extrapolated values to zero-pulse strengths and depend on the applied magnetic field H. References are given in the last column together with information on the doping. Data for the absorption α and corresponding oscillator strengths f are given for the optical geometry chosen in this work.

Parameters	Eu site I	Pr site I	Pr site II	
λ_0(transition,air) (nm)	579.879	605.813	607.770	Reference 44
$\Gamma_{LT}=1/(2\pi T_1)$ (Hz)	80	970	720	References 46 and 29
Γ_{inh} (GHz)	2.5	7	3	Multidoped [a]
$\Gamma_h(H=0)$ (Hz)	210			Single doped [b]
$\Gamma_h(H=0)$ (Hz)	195			Reference 14 [c]
$\Gamma_h(H=100$ G) (Hz)	105			Reference 14
$\Gamma_h(H=0)$ (Hz)		2400	1050	Reference 29 [d]
$\Gamma_h(H=80$ G) (Hz)		1800	850	Reference 29
$\Gamma_h(H=0)$ (Hz)	330	1650	1000	Multidoped
$\Gamma_h(H>500$ G) (Hz)		1200	900	Multidoped
α (cm^{-1})	2.7	1.4	0.18	Multidoped
f [e]	5.3×10^{-8}	7.7×10^{-7}	4.5×10^{-8}	Multidoped
μ (D) [f]	2.0×10^{-3}	7.5×10^{-3}	1.9×10^{-3}	Multidoped
$\lvert\Delta\nu_0/E_{ext}\rvert$ (kHz/V cm^{-1})	35 [g]	110	90	References 53 and 52
$\lvert\delta\mu\rvert$ [h] (D)	2.3×10^{-2}	7.3×10^{-2}	6.0×10^{-2}	

[a] 0.1 at. % Eu^{3+}: 0.01 at. % Pr^{3+}.
[b] 0.1 at. % Eu^{3+}.
[c] 0.1 at. % Eu^{3+}, different crystal.
[d] 0.02 at. % Pr^{3+}.
[e] Oscillator strength along electromagnetic field polarization.
[f] Vacuum value for $\epsilon(\omega_0)=1.8$ (Ref. 51).
[g] $\lvert\Delta\nu_0/E_{ext}\rvert\simeq17$ kHz/(V cm^{-1}) for Eu^{3+} site II.
[h] Vacuum value for $\epsilon(0)=7$.

and the characteristic dependence of the echo decay as a function of the excitation pulses is calculated.

The paper is structured as follows. In Sec. II the experimental setup and the experimental conditions are presented. In Sec. III, the broadening by various dynamical processes is discussed. Closing remarks are given in Sec. IV.

II. EXPERIMENT

The experimental setup is schematically illustrated in Fig. 1. The laser beam from a single-frequency tunable dye laser (CR 699-21) was chopped by two acousto-optic modulators (AOM) (Matshusita EFLM 200) to generate excitation pulse with typical lengths of 0.7–1.5 μs. The AOM driver (Brimrose VFA 200-75-B1-F1.25-E) allowed for fast frequency shifting of up to 50 MHz/50 ns. Using an additional electro-optic modulator (EOM) (Leysop driven by a New Focus high voltage amplifier 3211) the pulse amplitudes were independently controlled. Beams of powers up to 30 mW were focused by a 120-mm focal length lens onto the crystal resulting in a beam waist of approximately 45 μm. In some cases a focal length of 1 m was used.

The experiments were carried out on a $5\times5\times5$ mm^3 0.1 Eu^{3+}:0.01 Pr^{3+}:0.01 Nd^{3+} at. % codoped Y_2SiO_5 crystal.[40] The pulse propagation direction was chosen close to one of the crystal axes and the light polarization was adjusted to the maximum absorption.

The use of a multiply doped crystal proved to be very useful because it allowed for the measurement of different broadening effects in one and the same system. The laser wavelength was tuned either to the $^7F_0$-$^5D_0$ site-I transition at 579.879 nm of Eu^{3+} or to either site I or site II of the $^3H_4$-$^1D_2$ transition of Pr^{3+} at 607.773 nm or 605.813 nm, respectively.[44,29,45] To avoid persistent hole burning, the laser was repetitively scanned over a 400-MHz range in 250 ms. The echo signal, after passing through AOM 3 was detected by a photomultiplier (Hamamatsu 928) and recorded using boxcar integration. The residual background was additionally recorded for each t_{12} by switching off the first of the two excitation pulses. In this way the effect of hole burning and of slow baseline drifts could be eliminated. Averages were taken over 100 echoes at each time delay. The pulse power was synchronously monitored in order to control power drifts. All experiments were carried out at a temperature of 1.7 K. Results obtained in this work along with data taken from the literature are listed in Table I.

III. LINE-BROADENING MECHANISMS

In this section we discuss the broadening by the various dynamical processes as schematically presented in Eq. (2). These processes we classify as follows: (i) the broadening limited by the lifetime, (ii) lattice vibrations treated as equilibrium and nonequilibrium phonons, and (iii) TLS, SI, and EFS mechanisms related to the sudden-jump model.

A. Lifetime limits, equilibrium phonons, and TLS

The $^7F_0$-$^5D_0$ transition of Eu^{3+} in Y_2SiO_5 has been repeatedly investigated, the main objective being its very small

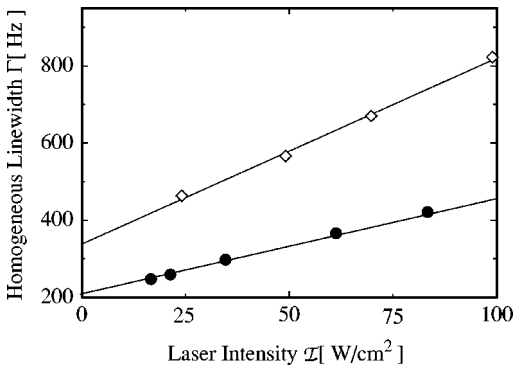

FIG. 2. Linewidth of the Eu^{3+} site I transition in Y_2SiO_5 for two crystals grown by flame fusion. The diamonds and circles are for a multiply doped and a singly doped crystal, respectively. In both cases the concentration of the Eu^{3+} ions is 0.1 at. %. Straight lines are linear fits to the data. Note the difference in the extrapolated zero-energy values.

lifetime-limited broadening of $\Gamma_{LT} \simeq 80$ Hz in site I.[46] A homogeneous linewidth close to this limit, $\Gamma_h \simeq 105$ Hz,[14] has been obtained. For the $^3H_4$-$^1D_2$ transition of Pr^{3+} the lifetime limited linewidths are considerably larger but still in the sub-kHz range, namely, $\Gamma_{LT} \simeq 970$ and 720 Hz for site I and site II, respectively.[44,29]

The line broadening by thermal phonons was measured for Eu^{3+} in Y_2SiO_5 by Altner *et al.*[32] A T^7 dependence was observed, which indicates that the broadening is governed by a Raman-type process. An onset of the broadening was recorded at temperatures >8 K. Thus for temperatures of $T \simeq 1.7$ K in the present work the broadening by equilibrium phonons can be disregarded. Referring to the work of Flinn *et al.* mentioned above,[18] the broadening extrapolated to zero temperature may change by two orders of magnitude depending on the technique applied for the crystal growth. It is thus not surprising that the linewidths measured for crystals grown under nominally identical conditions may also significantly differ from each other because the crystals are not identical. A minor change in the crystal quality may lead to a measurable change in the width.

In Fig. 2 the linewidths are shown for Eu^{3+} site I diluted in two Y_2SiO_5 crystals. Both crystals were grown by the flame-fusion method for equal concentrations of Eu^{3+} ions. Assuming a linear dependence on the pulse energy, the extrapolated zero-energy linewidths are 210 and 330 Hz. The smaller of the two values is consistent with the 195 Hz recorded without magnetic field by Equall *et al.*[14] Inspired by the measurements of Flinn *et al.*[18] and assuming a gradual change from a crystalline towards a glassy-type behavior with increasing disorder, we attribute the differences in the linewidth to the TLS dynamics. This conjecture is supported by the following reasoning. The differences of some hundreds of Hz between the broadenings of different crystals are small, if compared with the inhomogeneous broadening on scales larger by six orders of magnitude. The latter broadening also results from lattice imperfections. Only a marginal part of these imperfections has to undergo dynamics so that fluctuations of the order of kHz arise in the transition frequency. We believe that TLS are a possible reason for the differences between broadening data of the present study and of the literature given in Table I.

Concerning the temperature dependence, a linear increase is expected for Γ_{TLS} according to the standard TLS model. Correspondingly, the overall temperature dependence would follow a superposition of the linear and the T^7 law. Such a superposition is difficult to trace from experimental data because the T^7 law is only approximate and especially because the broadening by TLS is expected to be small and may thus be masked by stronger effects, as discussed below.

B. Spin-ion interactions

Spin-ion interactions have been analyzed in terms of the sudden-jump model that was initiated by Klauder and Anderson[15] and was extended by Hu and Hartman[25] and by Hu and Walker.[26] In this model the ions involved in the echo process interact magnetically with randomly flipping host spins. These interactions lead to fluctuations of the transition frequency and correspondingly to a dephasing. According to Eq. (27) of Ref. 26 the 2PPE intensities are

$$-\ln\left(\frac{I}{I_0}\right)_{SI} = c_{SI} e^{-x} \int_0^x \tilde{I}_0[\tilde{\xi}(x-x')]x'[\tilde{I}_0(x') + \tilde{I}_1(x')]dx', \tag{3}$$

where

$$\tilde{\xi} = \frac{k_1 - k_2}{k_1 + k_2}, \quad x = (k_1 + k_2)t_{12}. \tag{4}$$

c_{SI} is a constant and $\tilde{I}_j$ denotes the modified Bessel function of the first kind and of argument j. k_1 and k_2 in Eq. (4) are rates of the up- and down-spin flips. In the high-temperature limit $\tilde{\xi} = 0$ and one has for the asymptotic behavior

$$\ln\left(\frac{I}{I_0}\right)_{SI} \sim \begin{cases} -t_{12}^2 & , \quad t_{12}/T_m \ll 1 \\ -\sqrt{t_{12}} & , \quad t_{12}/T_m \gg 1, \end{cases} \tag{5}$$

where $k_1 = k_2 = T_m^{-1}$, with T_m denoting the spin flip time. From Eq. (5) it follows that with increasing t_{12} the echo intensity undergoes a crossover between the two asymptotic behaviors, as schematically shown in Fig. 3. We will make use of expression (3) in the next subsection.

C. Excitation-induced frequency shifts

One of the major attempts in this paper is to calculate the echo attenuation by EFS from first principles. Based on off-diagonal interactions, similar calculations have already been undertaken by Root and Skinner.[36] However, their predicted line broadening was by two orders of magnitude too small when compared with the experimental observations by Macfarlane and Shelby.[4] Our analysis strongly indicates that for the systems studied here, EFS results predominantly from diagonal interactions. To discriminate between the two types of interactions, we first derive approximate expressions for the echo attenuation due to these interactions. We then report on a particular experiment that allows for the distinction between the two effects and calculate the broadening by EFS from first principles.

Our approach is based on a statistical description of the excitations and is motivated by the sudden-jump model introduced for the spin dynamics. The dynamics of excitation

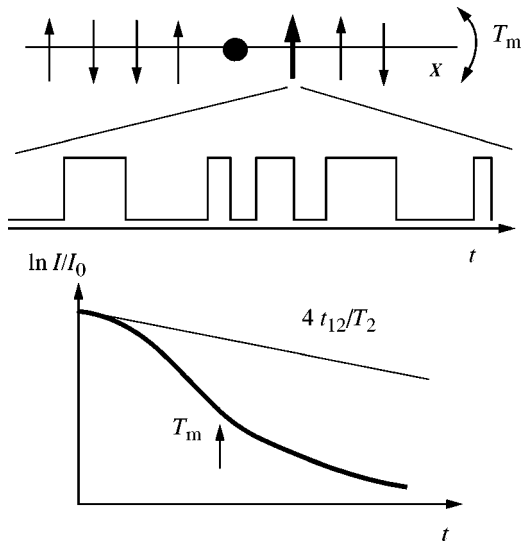

FIG. 3. Schematic representation of the sudden-jump model. The arrows denote up and down states of the spins located for simplicity on a one-dimensional lattice. The flips occur randomly at a rate T_m^{-1} for which a temporal realization is illustrated by the telegrapher's function for one spin. The ion, indicated by the dot, interacts with the spins, so that the the flips give rise to fluctuations in the ion's transition frequency. In the lower part the attenuation by spin-ion interaction is schematically depicted. The thin line represents the intrinsic broadening and the thick line includes the spin-ion interaction. A crossover is expected at $t_{12}=T_m$.

and deexcitation is treated as sudden events equivalent to the sudden spin flips. In this picture the sudden-jump and EFS model differ only by the nature of interaction and by the temporal realization of the dynamics. The approach is therefore semiclassical in the sense that the ions are considered as quantum two-level systems interacting with classical fields induced by spins and excitations.

Although well documented in the literature, we briefly give the definitions of the two types of interactions. We consider single-ion wave functions ϕ_{gj} and ϕ_{ej} for the electronic ground and excited states of an ion located at site j and ignore hyperfine splittings. From these basis functions the interactions between two ions are of the diagonal type:

$$\langle \phi_{xj}\phi_{yk}|\hat{V}|\phi_{xj}\phi_{yk}\rangle, \quad x,y\in\{g,e\}, \tag{6}$$

where $\hat{V}$ is the operator of the electronic interaction. The combination of the four integrals of this type leads to the shift in the transition frequency of one ion due to the excitation of another ion.[32] For the off-diagonal term we write[47]

$$J_{jk}=\langle \phi_{ej}\phi_{gk}|\hat{V}|\phi_{gj}\phi_{ek}\rangle. \tag{7}$$

To lowest order, the two-center expansion results in dipole-dipole interactions. For the calculation of the diagonal and the off-diagonal interactions static dipole-moment differences and transition-dipole moments, respectively, are used.

1. EFS by diagonal interactions

In Ref. 32 EFS was studied for the case where a high excitation density is induced by a third scrambler pulse. We extend this analysis to the case where the high excitation density is generated by the two echo inducing pulses. We write for the time-dependent electronic transition frequency $\omega_j(t)$ of the jth ion

$$\omega_j(t)=\omega_{0j}+\sum_k{}' D_{jk}\xi_k u_k(t), \tag{8}$$

where the sum runs over all lattice sites, except j (indicated by the prime). ω_{0j} is the ion static transition frequency at site j. The ω_{0j} frequencies are assumed to be distributed according to the inhomogeneous broadening; spatial correlation of the site energies is not considered here.[36] D_{jk} in Eq. (8) is the frequency shift induced by the excitation of the ion at a displacement $\mathbf{r}_{jk}$. The $\xi_k u_k(t)$ term is introduced to account for the randomness of ion positions and for the stochastic nature of the ion excitations. ξ_k is a variable indicating whether the kth site is occupied:

$$\xi_k=\begin{cases}1, & \text{with probability } p,\\ 0, & \text{with probability } 1-p,\end{cases} \tag{9}$$

where p denotes the probability of a lattice site to be occupied by a guest ion. $u(t)$ in Eq. (8) is considered to be a stochastic variable taking values 0 and 1 for the electronic ground and excited state of the ion, respectively. The state of the ion depends on the transition probability, the pulse energies, and the offset Δ between the laser and the transition frequency. As discussed in Appendix A, we denote by w_1 the excitation probability right after the first pulse and by w_2 the probability of changing state upon the second pulse. We take into account that the pulse times are short if compared with the interpulse time t_{12} so that damping during the pulse periods can be disregarded. We thus can write

$$\begin{aligned}&\text{Prob}[u(t)=1]\\ &\simeq\begin{cases}w_1 e^{-\gamma t}, & 0<t<t_{12},\\ w_1(1-2w_2)e^{-\gamma t}+w_2 e^{-\gamma(t-t_{12})}, & t_{12}<t<2t_{12}.\end{cases}\end{aligned} \tag{10}$$

The probability for $u(t)=0$ results from $\text{Prob}[u=0]=1-\text{Prob}[u=1]$. γ in Eq. (10) is the inverse lifetime $\gamma=1/T_1$ and is considered to be independent of the lattice site. w_1 and w_2 depend on the frequency offset Δ and the averages have to be taken over the inhomogeneous line shape. According to Appendix A for weak laser pulses

$$\langle w_{1,2}\rangle\simeq c\mathcal{T}_{1,2}, \quad c=\frac{1}{4\sqrt{2\pi}\sigma_\nu}, \tag{11}$$

where σ_ν is the standard deviation of the inhomogeneously broadened band in units of Hz. $\mathcal{T}_{1,2}$ denote the pulse energies $\mathcal{T}_{1,2}=\chi_{1,2}^2\tau_{1,2}$, with $\chi_{1,2}$ and $\tau_{1,2}$ being the Rabi frequencies and pulse times, respectively. According to Eqs. (1) and (8) the accumulated phase of the jth ion is given by

$$\int_0^{t_{12}}\omega_j(t)dt-\int_{t_{12}}^{2t_{12}}\omega_j(t)dt=\sum_k{}' D_{jk}\xi_k\theta_k, \tag{12}$$

where

$$\theta_k = \int_0^{t_{12}} u_k(t)dt - \int_{t_{12}}^{2t_{12}} u_k(t)dt, \tag{13}$$

is a random variable through the stochastic nature of $u(t)$ and depends on the offset Δ. Inserting Eq. (12) and Eq. (13) into Eq. (1) we find

$$P(t_{12}) = P_0 \prod_k{}' \langle \exp(iD_{jk}\xi_k\theta_k)\rangle_{\xi_k,\theta_k,\Delta}, \tag{14}$$

where the average is taken over the site occupations ξ_k, over the temporal realizations of θ_k, and over the distribution of the offset Δ. For small p values, one has[48]

$$P(t_{12}) \simeq P_0 \exp\left\{ -p \sum_k{}' [1 - \langle \exp(iD_{jk}\theta_k)\rangle_{\theta_k,\Delta}] \right\}. \tag{15}$$

In the dipole-dipole approximation the ion-ion interaction is given by

$$D_{jk} = (r_0/|\mathbf{r}_{jk}|)^3 \kappa(\Omega_{jk}) D_0. \tag{16}$$

D_0 represents the interaction between two dipoles at a unit distance r_0,

$$D_0 = \eta(0)\frac{(\delta\mu)^2}{4\pi\epsilon_0\hbar r_0^3}, \tag{17}$$

where $\delta\mu$ is the static dipole-moment difference of the electronic ground and excited states and $\epsilon_0 = 8.854\times 10^{-12}$ As/(V m). $\eta(\omega)$ in Eq. (17) stands for the dielectric correction that we write as[49]

$$\eta(\omega) = \frac{1}{\epsilon(\omega)}\left(\frac{\epsilon(\omega)+2}{3}\right)^2, \tag{18}$$

where $\epsilon(\omega)$ is the dielectric constant of the host medium at frequency ω. $\kappa(\Omega_{jk})$ in Eq. (16) gives the angular dependence of the interaction $\kappa(\Omega_{jk}) = (\widehat{\delta\mu}_j, \widehat{\delta\mu}_k) - 3(\hat{r}_{jk}, \widehat{\delta\mu}_j)(\hat{r}_{jk}, \widehat{\delta\mu}_k)$, where $\widehat{\delta\mu}$ and $\hat{r}$ are unit vectors for the dipoles and the displacement, respectively, and Ω denotes the set of angles defining the corresponding spatial orientations. In the continuum approximation,[32] Eq. (15) reads

$$\begin{aligned}\ln|P(t_{12})/P_0| &\simeq -4\pi\rho_0 p\left\langle \int_0^\infty dr r^2 \{1 - \cos[D_0\kappa(\Omega)(r_0/r)^3\theta]\}\right\rangle_{\theta,\Omega} \\ &= -C_1\langle|\theta|\rangle,\end{aligned} \tag{19}$$

where ρ_0 is the density of sites that can substitutionally be occupied by RE ions. Only the absolute value of the polarization is considered in Eq. (19) since the echo intensity $I \sim |P|^2$. The constant C_1 is equal to $(2/3)\pi^2 r_0^3 \rho_0 p\langle|\kappa|\rangle_\Omega D_0$, where the dimensionless quantity $\langle|\kappa|\rangle_\Omega$ is of the order 1. For the particular case, where all dipoles are parallel, $\langle|\kappa|\rangle_\parallel = 4/\sqrt{27}$, and when all dipoles are perpendicular with respect to the dipole at the origin $\langle|\kappa|\rangle_\perp = 2/\pi$.[32]

The derivation of $\langle|\theta(t)|\rangle$ as a function of the excitation probabilities is given in Appendix B. Making use of Eqs. (19) and (B9) we obtain for the echo intensity

$$\ln\left(\frac{I}{I_0}\right)_{\text{EFS-D}} \simeq -2C_1\gamma^{-1}[\langle w_1(1-w_2)\rangle(1-e^{-t_{12}\gamma})^2 + \langle w_2\rangle(1-e^{-t_{12}\gamma})], \tag{20}$$

where we used the subscript EFS-D to indicate EFS by diagonal interactions. For weak pulses we have

$$\ln\left(\frac{I}{I_0}\right)_{\text{EFS-D}} \simeq -2cC_1\gamma^{-1}[\mathcal{T}_1(1-e^{-t_{12}\gamma})^2 + \mathcal{T}_2(1-e^{-t_{12}\gamma})]. \tag{21}$$

Writing for the echo intensity $\ln(I_{\text{echo}}/I_0) = -4t_{12}/T_2$, the broadening Γ in units of Hz is related to the dephasing time T_2 by $\Gamma = (1/\pi T_2)$. For $\gamma t_{12} \ll 1$ and from Eq. (21) the broadening is therefore

$$\Gamma_{\text{EFS-D}} \simeq \frac{1}{2\pi} C_1\langle w_2\rangle \simeq \frac{1}{2\pi} cC_1\mathcal{T}_2, \tag{22}$$

where the latter equality holds for weak pulse strengths. We thus have found that for short t_{12} the broadening depends predominantly on the energy of the second pulse, in agreement with previous results.[8,5,10,14,11] This behavior is regarded as a signature of the broadening by EFS in 2PPE.

2. EFS by off-diagonal interactions

EFS by off-diagonal interactions were studied by Root and Skinner[35,36] using a cumulant expansion technique. Here we apply a slightly different method that has been inspired by the analysis of EFS by diagonal interactions. The treatment of the full problem is involved. We therefore approximate the fully coupled system by sums of independent ion-pair interactions. For each pair we calculate independently the frequency shifts from the diagonalization of a two-by-two problem. The transition frequency of the jth ion is then

$$\omega_j(t) \simeq \omega_{0j} + \sum_k{}' \xi_k(1-u_k(t))\sigma_{jk} \times [\sqrt{J_{jk}^2 + (\Delta_{jk}/2)^2} - |\Delta_{jk}/2|], \tag{23}$$

where $\Delta_{jk} = \omega_{0j} - \omega_{0k}$ and $\sigma_{jk} = \text{sgn}(\omega_{0j} - \omega_{0k})$. ξ_k and $u_k(t)$ have the meaning as in Eq. (8). The term $1-u_k(t)$ indicates that the off-diagonal interaction arises when the kth ion is in the ground state. For $|J_{jk}/\Delta_{jk}| \ll 1$ we note that the lowest-order expansion of the term in rectangular brackets in Eq. (23) corresponds to the perturbation calculation of second order applied to the full problem. The calculation of expectation values is complicated because the averaging includes the conditional probabilities of site j and k excitations separated by the frequency Δ_{jk}. To simplify the calculations we assume that the frequency of site j coincides with the laser frequency and that the frequency Δ_{jk} is either fixed to a value $|\Delta\omega_s|$ if a high excitation density is generated with a scrambler pulse shifted in frequency by $\Delta\omega_s$ or is restricted to the range $[-\Delta_{\max}, \Delta_{\max}]$ that corresponds to spectral width of laser excitation. $\Delta_{\max}$ is thus approximately $\Delta_{\max}$

$\simeq \max\{\chi, \Delta_{\text{laser}}/2\}$, where χ and Δ_{laser} denote the Rabi frequency and the spectral width of some average pulse, given by the pulse-width limit or the laser jitter, respectively. The spectral density is considered to be constant within the range $[-\Delta_{\max}, \Delta_{\max}]$ because $\Delta_{\max}$ is much smaller than the inhomogeneous linewidth Γ_{inh}. Similarly to the previous derivations we find for the polarization

$$-\ln(P(t_{12})/P_0) \simeq p \sum_k{}' \, (1 - \langle \exp\{-i\theta_k \sigma_{jk}[\sqrt{J_{jk}^2 + (\Delta_{jk}/2)^2} - |\Delta_{jk}/2|]\}\rangle_{\theta_k, \Delta_{jk}}), \tag{24}$$

where θ_k is given in Eq. (13) and where the average is also taken over the distributions of the Δ_{jk}. Furthermore,

$$J_{jk} = J_0 \kappa(\Omega_{jk})(r_0/|\mathbf{r}_{jk}|)^3, \quad J_0 = \eta(\omega_0)\frac{\mu^2}{4\pi\epsilon_0 r_0^3 \hbar}. \tag{25}$$

Here μ denotes the transition dipole moment and the dielectric correction $\eta(\omega_0)$ of Eq. (18) is given for the transition frequency ω_0. Approximate expressions of Eq. (24) are derived in Appendix C. From Eqs. (C7) and (C12) we obtain

$$\ln\left(\frac{I}{I_0}\right)_{\text{EFS-J}} \simeq \begin{cases} -2C_2\langle|\theta|\rangle, & t_{12}\Delta_{\max} \ll 1, \\ -2^{3/2}C_2 \dfrac{\langle|\sqrt{\theta}|\rangle}{\sqrt{\pi\Delta_{\max}}}, & t_{12}\Delta_{\max} \gg 1, \end{cases} \tag{26}$$

where $C_2 = (2\pi^2/3) J_0 p r_0^3 \rho \langle|\kappa|\rangle$ and EFS-J indicates EFS by off-diagonal interactions. For small $t_{12}\gamma$ we have $\langle|\theta|\rangle \simeq \langle w_2\rangle t_{12}$, according to Eq. (B11), and we similarly approximate $\langle\sqrt{|\theta|}\rangle \simeq \langle w_2\rangle \sqrt{t_{12}}$. Thus with increasing t_{12} we expect a crossover from linear to square-root behavior. As in Eq. (22) for $t_{12}\gamma \ll 1$ we write

$$\Gamma_{\text{EFS-J}} \simeq \frac{1}{2\pi} C_2 \langle w_2\rangle \simeq \frac{1}{2\pi} c C_2 \mathcal{T}_2, \tag{27}$$

where again the latter equality holds for a weak second pulse. Interestingly, the condition $t_{12}\Delta_{\max} \ll 1$ in Eq. (26), required for an exponential decay, is unlikely to be satisfied in 2PPE. For the pulse-time-limited width, one has $\Delta_{\max} \simeq \pi/\tau$ and consequently the exponential decay is limited to the regime $t_{12}/\tau \leqslant \pi$. Thus, primarily the square-root behavior should be observed. Nevertheless, Eq. (27) may serve as an upper bound for the EFS broadening by off-diagonal interactions.

3. Quantitative determination of the broadening contributions

In order to investigate how diagonal and off-diagonal interactions contribute to the line broadening we have designed a particular experiment. The scheme of this experiment was inspired by Eq. (26) and by the investigations in Refs. 5, 6, 10, and 11, where with an extra laser pulse a high excitation density is induced in the system. The timing and laser frequencies are schematically shown in the upper part of Fig. 4. With two weak pulses the echo is generated, while with a third, scrambler pulse in the rephasing period, a strong excitation density is induced. The scrambler pulse is chosen to be in the rephasing period to maximize the broadening

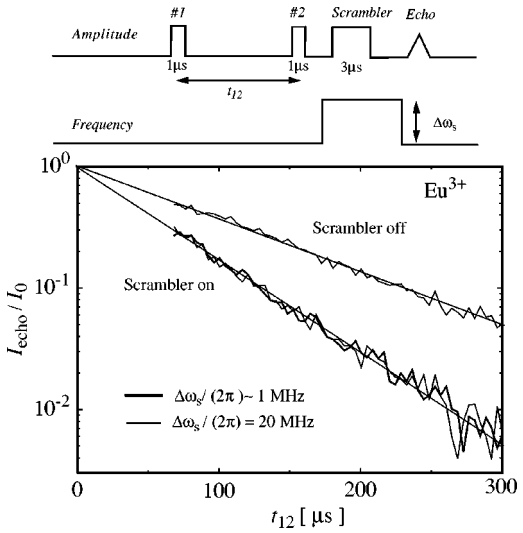

FIG. 4. Echo intensities as a function of the scrambler excitations for Eu^{3+} in Y_2SiO_5. In the upper part of the figure the timing of the pulses and the excitation frequencies are depicted. The scrambler pulse is applied at the time t_s in the rephasing period at a frequency shifted by $\Delta\omega_s$. In the lower part the echo intensities are plotted with the scrambler pulse set off and on. The straight lines are guides to the eye. The fact that there is no dependence on the frequency offset $\Delta\omega_s$ suggests that EFS by off-diagonal interactions is negligible.

effect. To examine whether there is a dependence of the echo on the scrambler frequency, the frequency of the third pulse is shifted by $\Delta\omega_s$.

For the data of Eu^{3+} in Y_2SiO_5, shown in Fig. 4, the echo intensity was recorded as a function of t_{12} without and with scrambler pulse. In the latter case the time interval between the second and the third pulse was kept fixed. The scrambler pulse energy was chosen to be three times stronger than the echo pulses. In a third case the scrambler pulse was shifted by $\Delta\omega_s/2\pi = 20$ MHz, a shift clearly larger than the Rabi frequency and the laser jitter of approximately 1 MHz. For the predictions, Eq. (26) has to be modified by replacing $\Delta_{\max}$ by $|\Delta\omega_s|$ in the case where $|\Delta\omega_s| > \Delta_{\max}$. Furthermore, we set $\langle|\theta|\rangle \simeq \langle w_3\rangle(2t_{12} - t_s)$, where t_s denotes the time instance of the scrambler pulse, again assuming a δ-shaped pulse. Here $\langle w_3\rangle$ is the excitation probability of the scrambler pulse. Correspondingly, we approximate $\langle\sqrt{|\theta|}\rangle \simeq \langle w_3\rangle\sqrt{2t_{12} - t_s}$. The experimental data suggest that in all three cases only a linear behavior of $\ln(I/I_0)$ is present. Furthermore, up to the experimental accuracy the echo intensity does not depend on the offset $\Delta\omega_s$. These observations indicate that off-diagonal interactions are negligible for the broadening in the present system.

For the quantitative predictions of the broadening by EFS we first compare the broadening by diagonal and off-diagonal interactions. We consider the ratio R of the two broadenings, Eqs. (22) and (27). Because the two terms are very similar the ratio is of the simple form

$$R \equiv \frac{\Gamma_{\text{EFS-J}}}{\Gamma_{\text{EFS-D}}} = \frac{\eta(\omega_0)\mu^2}{\eta(0)(\delta\mu)^2}, \tag{28}$$

where, recalling, μ and $\delta\mu$ are the transition dipole moment and the static dipole moment difference. We determined μ

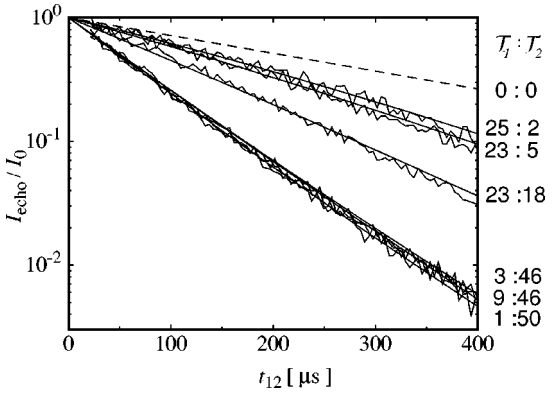

FIG. 5. Echo attenuation by EFS for Eu^{3+} site I in Y_2SiO_5. Plotted are the experimental echo intensity for various pulse energies as a function of t_{12}. The relative energies $\mathcal{T}_1, \mathcal{T}_2$ of the first and second pulses are as indicated. The full smooth lines give the calculations according to Eq. (21) with a single cC_1 value taken as a fitting parameter. The dashed line corresponds to the zero-energy-extrapolated broadening, $\Gamma_h = 330$ Hz.

from the oscillator strength f using the expression

$$\mu^2 = \frac{3\hbar e^2 f}{2\omega_0 m_e} \frac{9\sqrt{\epsilon(\omega_0)}}{[\epsilon(\omega_0)+2]^2}, \tag{29}$$

where f denotes the oscillator strength of the transition in the solid along the electromagnetic field polarization. f was determined independently from absorption intensities measured for the same laser polarization and crystal orientation that were used in the current experiments assuming equal guestion concentrations in the two inequivalent sites. The second ratio in Eq. (29) is the dielectric correction that accounts for μ being the dipole moment in the vacuum.[50] $\epsilon(\omega_0)$ is the dielectric constant at the transition frequency ω_0 that we calculated from the refractive index $n(\omega_0) \simeq 1.8$.[51] $\delta\mu$ was determined from independent experiments. The Stark shifts $|\Delta\nu_0 / E_{ext}|$ were measured using Stark-modulated photon echoes[52] and by means of electric-field-induced splittings of spectral holograms, using an actively stabilized laser system with a linewidth of 5 kHz.[53] Here $\Delta\nu_0$ denotes the electric-field-induced shift of the transition frequency and E_{ext} is the externally applied electric field. From these shifts we calculate the dipole moments as

$$|\delta\mu| = \frac{3h}{\epsilon(0)+2} \left| \frac{\Delta\nu_0}{E_{ext}} \right|, \tag{30}$$

where the Lorentz field factor accounts for the dielectric correction.[54] We are not aware of experimental $\epsilon(0)$ data for Y_2SiO_5. We thus have estimated $\epsilon(0) \simeq 7$ from values of similar crystals. The values of f, μ, $|\Delta\nu_0/E_{ext}|$, and $|\delta\mu|$ are collected in Table I. Based on these dipole moments we calculated the ratio R of Eq. (28) as 5×10^{-3}, 8×10^{-3}, and 7×10^{-4} for Eu^{3+} site I, Pr^{3+} site I, and Pr^{3+} site II, respectively. These ratios indicate very strongly that in this system the broadening by off-diagonal interactions is much smaller than that caused by diagonal interactions. This finding is in agreement with the results of the particular experiment discussed above and presented in Fig. 4. It is furthermore supported by the observation of Root and Skinner, although for a different system, that the predictions based on off-diagonal interactions are significantly smaller than the experimentally measured broadening.[36] We therefore restrict the further analysis of EFS to diagonal interactions.

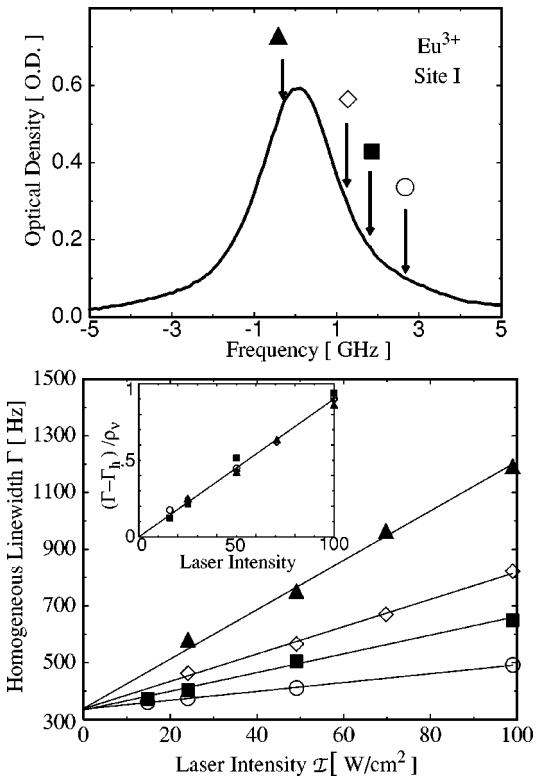

FIG. 6. Line broadening as a function of the position in the inhomogeneously broadened band of Eu^{3+} in Y_2SiO_5. The figure on the top depicts the four frequency positions ν in the inhomogeneously broadened band. In the figure on the bottom the linewidths are plotted for these positions as functions of the laser intensity. All curves yield the same extrapolated value $\Gamma_h = 330$ Hz that is also used in Fig. 5. The inset shows $(\Gamma - \Gamma_h)$ rescaled by the line profile $\rho_\nu(\nu)$ on an arbitrary scale. The data collapse indicates that the broadening depends solely on the excitation density in the system. The straight lines correspond to linear fits.

We compare the predicted behavior of broadening by EFS with the experimental data and concentrate first on the measurements of Eu^{3+} ions. Typical attenuation decays are shown in Fig. 5 together with a fit of Eqs. (19) and (21) to the data using cC_1 as the only fitting parameter. The echo intensity depends predominantly on the energy of the second pulse in agreement with the predictions. We also note a weak tendency of the decay deviating from an exponential towards a more Gaussian behavior for a strong first pulse and towards stretched exponential behavior for a strong second pulse again in agreement with the predictions of Eq. (21) and with previous observations.[5]

We also investigated the echo attenuation depending on the frequency position in the inhomogeneously broadened band. The echo intensities were recorded as a function of the energy $\mathcal{T} = \mathcal{T}_1 + \mathcal{T}_2$ for fixed ratios $\mathcal{T}_1 : \mathcal{T}_2$. The results are shown in Fig. 6. From Eq. (21) it is obvious that the broadening by EFS depends linearly on the excitation density in the system. The experimental data of Fig. 6 are consistent with such a behavior. Upon rescaling of the laser-intensity-dependent broadening $(\Gamma - \Gamma_h)$ by $\rho_\nu(\nu)$, the spectral den-

sity at the corresponding frequency position, the data fall on top of each other, so that a data collapse results, as shown in the inset of Fig. 6. As a matter of fact, the extrapolation to small intensities gives the same limiting value of $\Gamma_h = 330$ Hz for all spectral positions. The data collapse confirms the conclusion that the broadening by EFS depends linearly on the excitation density in the system. The present results are in agreement with similar observations in Refs. 4,33,34, and 55.

However, the linear dependence of the broadening on the excitation density is not a unique feature of EFS by diagonal interactions. Root and Skinner[35,36] showed that the broadening by off-diagonal interactions also scales linearly with the concentration and used their approach for the interpretation of the experimental results of Macfarlane and Shelby.[4] For Pr^{3+}:LaF_3, Zhang and Mossberg[34] assigned the dependence of the broadening on the frequency position in the inhomogeneous band to EFS. A linear dependence is also expected for the broadening by NQP, as we shall see below. Therefore 2PPE measurements carried out at different positions in the inhomogeneous band neither allow for a discrimination between the two types of EFS interactions nor permit for the distinction between EFS or NQP broadening.

We now quantitatively determine the EFS broadening using electric-field data and exemplify the calculations for Eu^{3+} ions. Making use of Eqs. (17), (22), and (30) we find

$$\Gamma_{\text{EFS-D}} \simeq \frac{4\pi}{3\sqrt{27}} p \rho_0 r_0^3 \langle w_2 \rangle D_0 = \frac{2\pi h p \langle w_2 \rangle}{3\sqrt{27}\epsilon_0 \epsilon(0) r_0^3} \left| \frac{\Delta \nu_0}{E_{\text{ext}}} \right|^2 , \tag{31}$$

where we have considered the parallel case: $\langle |\kappa| \rangle_{\parallel} = 4/\sqrt{27}$. The dielectric correction has now reduced to the screening $1/\epsilon(0)$. p, as defined above, denotes the relative site-occupation probability that is calculated from the Eu^{3+}-ion concentration of 0.1 at. %, corresponding to 0.025 mol %. Thus $p \simeq 1.25 \times 10^{-4}$, where an extra factor of 1/2 has been introduced because the ions substitutionally occupy two optically distinct sites with equal probability. $\langle w_2 \rangle$ is estimated from the saturation effect observed for Pr^{3+} site I, as discussed below. We obtain $\langle w_2 \rangle \simeq 1.6 \times 10^{-4}$. The value of r_0 can be calculated from crystallographic measurements. For the monoclinic Y_2SiO_5 crystal the unit-cell parameters are $a = 10.42$ Å, $b = 6.72$ Å, $c = 12.49$ Å, $\beta = 102°$ with eight Y_2SiO_5 per unit cell.[45] We replace the actual lattice by a simple cubic lattice with the same atom density and find $r_0 \simeq 2.4$ Å for the corresponding lattice unit. ρ_0 is fixed by setting $\rho_0 r_0^3 = 1$. For the range $t_{12} \leqslant 400$ μs and $T_1 \simeq 2$ ms the condition $\gamma t_{12} \ll 1$ is obeyed so that Eqs. (22) and (31) are applicable. We calculate $\Gamma_{\text{EFS-D}} \simeq 650$ Hz for Eu^{3+} site I that compares with the experimental value of 850 Hz.

We compare the broadening by EFS for site I and site II of Eu^{3+} in Y_2SiO_5 using the experimental data of Equall *et al.*[29] From Fig. 2 of their paper we estimate the ratio site I : site II for the broadening by EFS to be 0.7. For the prediction we take into account the ratio site I : site II equal to 0.3 for the oscillator strengths given in the same paper and the corresponding ratio of the inverse inhomogeneous line broadening equal to 1.1, and further assume that both measurements were carried out in the band center. The ratio of the static dipole moments is calculated from the data in Table I. This yields an overall ratio site I : site II of 1.3 that compares with the predicted value of 0.7.

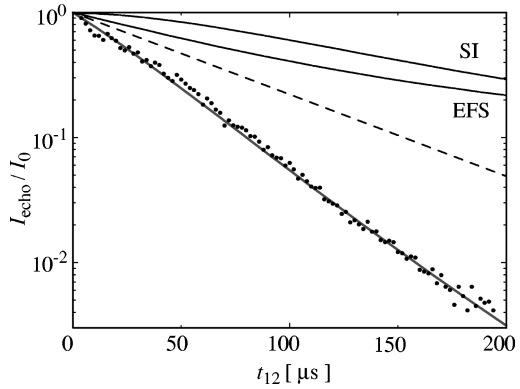

FIG. 7. Competing broadening mechanisms for Pr^{3+} site I in Y_2SiO_5. Plotted is a typical echo decay for a moderate laser intensity. The thick full line through the data is the fit. The thin dashed line gives the intrinsic broadening $\Gamma_h \simeq 1200$ Hz obtained from zero-energy extrapolation with the magnetic field set on. The thin full lines are the SI and EFS contributions. See text for details.

We now analyze the experimental echo decays observed in Pr^{3+} site I in Y_2SiO_5. The spin dynamics in Y_2SiO_5 is attributed to the ^{89}Y spins. The ^{29}Si spins are ignored because they are known to contribute less to the broadening by a factor 40.[46,29] This factor primarily results from the small, 4% isotope abundance of ^{29}Si. We also ignore frozen-core effects. From Table I we see that in the case of Pr^{3+} site I the difference in the homogeneous broadening with and without field is approximately $\Gamma_h(H=0) - \Gamma_h(H>500\text{G}) \simeq 450$ Hz. This difference was observed to be about five times smaller for Pr^{3+} site II and Eu^{3+} site I. We therefore approximated the spin-ion contribution by an exponential for the latter two as done in previous publications.[14,29] For Pr^{3+} site I, however, the broadening by SI is strong enough so that the nonexponentiallities according to Eq. (3) should be visible. In Fig. 7 a typical photon-echo decay for Pr^{3+} site I at intermediate pulse energies is shown along with the broadening by SI with $k_1 = k_2 = T_m^{-1}$, using Eq. (3), the broadening by EFS, and the intrinsic broadening Γ_0 exclusive to the SI contribution. From the figure it is clear that the nonexponential behavior by SI is weak and is partially masked by the competing effect through EFS. In the fit Γ_0 was set equal to $\Gamma_h \simeq 1200$ Hz, corresponding to the measured zero-energy-extrapolated broadening in an external magnetic field. The flip time T_m, and the prefactor for the broadening by EFS were adjusted to the experiment. The prefactor c_{SI} was fixed so that the SI contribution corresponded to the difference between the homogeneous widths with and without magnetic field. We obtained a flip time of $T_m \simeq 200$ μs. Because of the weak broadening by spin-ion interactions, and particularly because of the superposition of two effects, the value of T_m is only very approximate.

As demonstrated in Fig. 7 the echo decays deviate only weakly from the nonexponential behavior, especially for larger t_{12}. Therefore the data of Pr^{3+} site I were fitted to an exponential law for times $t_{12} > 20$ μs. The linewidths in Fig. 8 are given for a fixed ratio $2\mathcal{I}_1 : \mathcal{I}_2 = 1$ according to the ratio $\tau_1 / \tau_2 = 1/2$ and equal laser intensity $\mathcal{I}$ for the two pulses. As a function of the laser intensity $\mathcal{I}$ the experimental linewidths

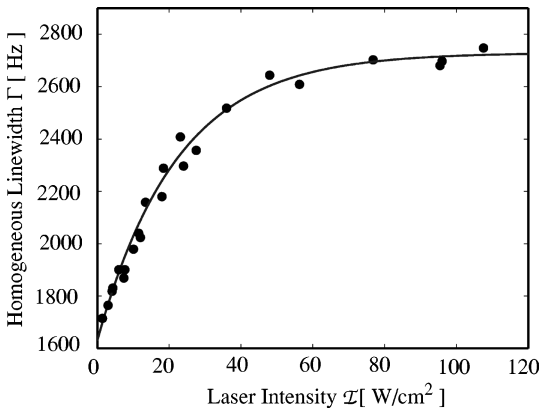

FIG. 8. Linewidths of Pr^{3+} site I in Y_2SiO_5 as a function of the laser intensity $\mathcal{I}$. The linewidths were measured without magnetic field and are given for a fixed ratio $2\mathcal{T}_1:\mathcal{T}_2=1$ of the pulse energies. The full line is the fit $\Gamma=\Gamma_h+A[1-\exp(-c_1\mathcal{I})]$, see text. The value extrapolated to zero power yields $\Gamma_h=1650$ Hz.

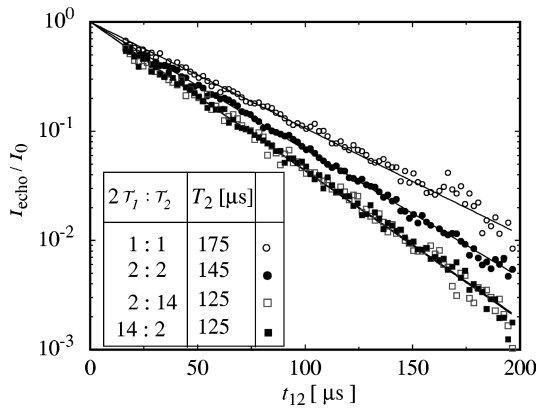

FIG. 10. Echo attenuation for Pr^{3+} site I in Y_2SiO_5. Plotted are the echo intensities as a function of t_{12} for several energies of the two pulses. The duration of the first pulse was chosen to be half of the second pulse duration. The ratios of the pulse energies are indicated in the inset as $2\mathcal{T}_1:\mathcal{T}_2$ for an arbitrary scale. The full lines are fits to the exponential law with the corresponding T_2 also given in the inset.

follow a linear behavior at low intensity and show saturation at large intensity. At saturation the observed broadening is 1100 Hz. The full line gives the fit of $\Gamma=\Gamma_h+A[1-\exp(-c_1\mathcal{I})]$, with A and c_1 as adjustable parameters. The figure indicates that the data monotonically approach the saturation value. The resolution of the data is probably too small for the detection of a maximum in the broadening, as predicted in Fig. 9. Equally well, laser-field inhomogeneities may be present so that the hump in the broadening is smoothed out, as discussed in Appendix A. In Fig. 10 echo intensities of Pr^{3+} site I are shown for different ratios $2\mathcal{T}_1:\mathcal{T}_2$. Because of the small relative broadening the t_{12} times had to be extended up to 200 μs in order to detect the pulse-energy-dependent broadening. This time scale is comparable to $T_1=165$ μs so that the $\gamma t_{12}\ll 1$ condition is not satisfied. Correspondingly, Eq. (21) has to be applied instead of Eq. (22), and a dependence of the echo also on the energy of the first pulse is expected. In fact, such a dependence can be observed in Fig. 10.

For comparison the echo intensity was also investigated for Pr^{3+} site II. The echo signal was weak if compared with

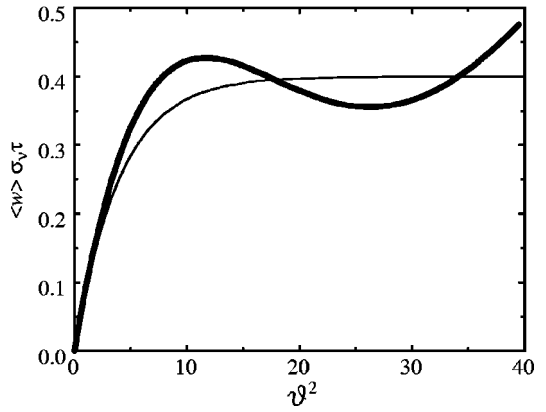

FIG. 9. Excitation density after a single pulse. Plotted is the averaged excitation probability as $\sigma_\nu\tau\langle w\rangle$ for the case of $\sigma_\nu \gg \chi$. The thick line gives the calculation of Eq. (A3). A maximum is observed at $\vartheta^2\simeq 11.5$. The thin line is $0.4[1-\exp(-2.5c\,\vartheta^2)]$, representing the approximate saturation behavior on the scale of $\vartheta^2 \leqslant 4\pi^2$. See Appendix A for details.

the site-I intensity because of the much smaller oscillator strength. No broadening effect could be observed up to a laser intensity of 100 W cm^{-2}. We conclude that the laser-intensity-dependent broadening is smaller than 100 Hz, which marks approximately the visibility limit. Independent measurements in a 0.1% Pr^{3+}:Y_2SiO_5 doped crystal showed that at higher concentrations an intensity-dependent broadening is present in accordance with the observations by Equall *et al.*[29]

As for Eu^{3+} we calculate the broadening for Pr^{3+} by taking into account the corresponding excitation densities, dipole moments, and ion concentrations. The calculation of the excitation probability $\langle w_2\rangle$ is based on the saturation behavior in the echo attenuation of Pr^{3+} site I. We compare the experimental saturation behavior in Fig. 8 with the calculated one in Fig. 9. From this comparison we estimate that in Fig. 9 the maximum of $\langle w\rangle$ at $\vartheta_2^2=11.5$ corresponds to the laser intensity of $\mathcal{I}\simeq 25$ W cm^{-2} in Fig. 8. The excitation probability in Fig. 9 saturates at a value of $\langle w\rangle\sigma_\nu\tau=0.4$ so that we find $\langle w_2\rangle\simeq 0.4/(\sigma_\nu\tau_2)\simeq 9.6\times 10^{-5}$ at saturation. According to Eq. (31) and the data of Table I we calculate $\Gamma_{\text{EFS-D}}\simeq 450$ Hz for Pr^{3+} site I, roughly a factor of 2 smaller than the experimentally observed 1100 Hz. For the the Rabi frequencies of Eu^{3+} and Pr^{3+} site II we consider the dependence of the Rabi frequency on the oscillator strength and the laser energy, $\chi^2\sim f\mathcal{T}$, and derive from $\vartheta_2^2=11.5$ for Pr^{3+} site I at $\mathcal{I}\simeq 25$ W cm^{-2} the corresponding values $\vartheta_2^2=3.2$ for Eu^{3+} and $\vartheta_2^2=2.7$ for Pr^{3+} site II at the laser intensity of $\mathcal{I}=100$ W cm^{-2}. From these parameters, making use of Eq. (A5), we find $\langle w_2\rangle\simeq 1.35\times 10^{-4}$ and 9.6×10^{-5} for Eu^{3+} and Pr^{3+} site II, respectively. The value of $\langle w_2\rangle\simeq 1.35\times 10^{-4}$ was applied above in the calculation of the broadening for Eu^{3+}. For Pr^{3+} site II we obtain $\Gamma_{\text{EFS-D}}\simeq 300$ Hz, which is by a factor of 3 larger than the visibility limit.

We conclude that for the systems under consideration the predicted values agree within a factor of 2 to 3 with the experimental results. We explain part of the discrepancies by uncertainties of the data used in the predictions. The dielectric constant $\epsilon(0)=7$ is only a guess and its anisotropic

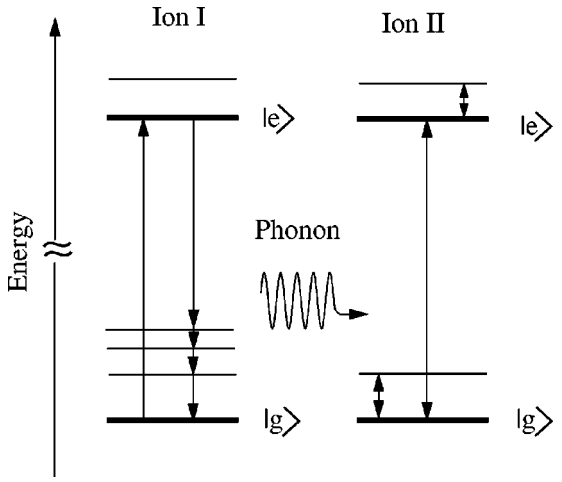

FIG. 11. Schematic representation of the echo attenuation by NQP. The excitation of ion I decays spontaneously and populates low lying electronic states. These populations decay by generating nonequilibrium phonons. Resonant and nonresonant scattering of the phonons at transitions in the ground and excited state of ion II lead to a dephasing in the electronic excitation.

properties are not considered at all. Furthermore, the effective concentration of the ion in the crystal might be different from the one given by the nominal weight percents. Finally, NQP may additionally contribute to the broadening as we shall discuss in the next section.

D. Nonequilibrium phonons

For the analysis of the echo attenuation by NQP the following independent processes have to be considered: the generation and relaxation of NQP, the propagation of the NQP in the solid, and the interaction between the NQP and the excitations involved in the echo process.

NQP are generated directly by spontaneous decays from the pumped electronic state to ground-state phonon modes by electron-phonon coupling. In the case where there are low-lying electronic states, these states may be populated by the spontaneous transitions and the population of these levels may then subsequently relax into NQP. The lifetime of NQP depends strongly on their frequency ν_p. For $\nu_p > 1$ THz the phonon lifetime τ_p limited by anharmonic relaxation was found to follow a $\tau_p \sim \nu_p^{-5}$ law.[56,57] Superimposed to this relaxation, if there are several low-lying electronic levels the NQP may more efficiently relax by repeated inelastic scattering so that eventually a large density of phonons resonant with the lowest electronic level is accumulated. This path is particularly feasible if the low-lying electronic levels are within the Debye frequency range. If there are several different ion species, the number of relaxation paths is increased and the lowest level out of all ion levels may act as a bottleneck so that NQP are accumulated at a frequency resonant with this level. Elastic scattering of NQP resonant with the lowest electronic state can occur many times before the NQP decay by anharmonic relaxation.

In the quasiparticle picture of phonon dynamics, the phonons are assumed to perform random walks through the crystal by elastic scattering and to relax by inelastic scattering. They are also scattered at electronically excited impurity

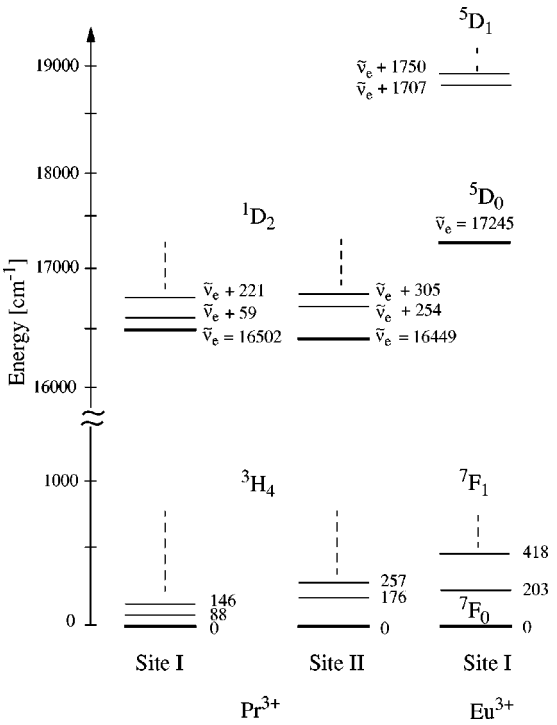

FIG. 12. Level scheme of Pr^{3+} and Eu^{3+} in Y_2SiO_5. The data are taken from Refs. 29,44,46 and 59; all energies are given in units of wave numbers. Only site I is depicted for Eu^{3+}. $\tilde{\nu}_e$ denotes the transition frequency to the state pumped by the laser. For the ground and the excited states the two closest-lying Stark levels are also indicated.

ions and these scattering processes give rise to a dephasing,[56,7,6] as schematically shown in Fig. 11. The dephasing is particularly efficient when electronic transitions of the ion involved in the echo process are resonant with the NQP. While these resonances are more likely for ground-state transitions, they might also occur for transitions in the excited state if the frequency gaps between the pumped state and higher electronic states are comparable to the phonon frequencies. In this case, depending on the electronic excitation density and the scattering cross sections, an accumulation of NQP resonant with these transitions may take place.

Resonances of NQP with transitions in the ground and the excited states lead to a lifetime shortening of the ground or excited state, respectively. These shortenings give rise to a dephasing in the excitation of an ion in the superposition state and thus to an echo attenuation. The efficiency of the attenuation by NQP is limited, apart from the phonon lifetime, by the time of detuning from the resonances and by the time at which the NQP diffuse out of the area probed by the laser.[6,58] Bai and Kachru interpreted their experimental results in terms of 51-cm^{-1} NQP, resonant with the lowest electronic state of Pr^{3+} in $YAlO_3$. Macfarlane and Meltzer,[7] as mentioned in the Introduction, pumped an electronic state 29 cm^{-1} higher than the state involved in the echo process with a second laser source. In this way NQP of 29 cm^{-1} were generated by phonon-assisted relaxation to the lower state. The increased broadening was attributed to the resonance with the 29-cm^{-1} NQP.

From the preceding considerations it is obvious that the broadening by NQP depends crucially on the electronic level

scheme of the ions. In Fig. 12 the level schemes of Pr^{3+} site I and site II and of Eu^{3+} site I are shown. For Pr^{3+} site I, the lowest Stark levels of the $^3H_4$ and of the $^1D_2$ states are separated by 88 and 59 cm^{-1}, respectively.[29] For Pr^{3+} site II, the corresponding energy gaps are significantly larger, namely, 176 and 200 cm^{-1} . For Eu^{3+} site I in the ground state, the lowest of the $^7F_1$ Stark levels is shifted by 203 cm^{-1} from the $^7F_0$ level.[46] In the excited state the closest-lying level is as far as 1707 cm^{-1} .[59] This situation is similar to that of Eu^{3+} site II with the corresponding transition at 580.049 nm. For Nd^{3+}, also contained in the present system, the lowest level is shifted by 91 and 68 cm^{-1} from the ground state for site I and site II.[32] We now discuss whether NQP might be of importance for Pr^{3+} site I where the 88-cm^{-1} level may be resonant with NQP. However, this level is higher than the 68 cm^{-1} state of Nd^{3+} site II, so that the latter level may act as a bottleneck. Even smaller is the 59 cm^{-1} transition of Pr^{3+} site I in the excited state so that this transition may also work as a bottleneck. We thus conclude that broadening by NQP is likely to occur for Pr^{3+} site I.

We estimate the broadening associated with NQP resonances from a collision model by making use of the expression $\Gamma_{\mathrm{NQP}} \simeq \sigma_0 v_p N_p/\pi$,[60] where σ_0 is the cross section for elastic scattering, v_p denotes the phonon velocity, and N_p is the density of phonons. We consider the data of Baumgartner *et al.*[56] obtained for CaF_2 and of Renk[58] measured for V^{4+}:Cr^{3+}:Al_2O_3. The resonant cross section is of the order $\sigma_0 \simeq 10$ nm^2. For inelastic scattering, the cross section is orders of magnitude smaller, depending on the energy mismatch. For the phonon velocity we consider $v_p \simeq 5 \times 10^3$ m/s. The phonon density we calculate from a steady-state approach,[6] $N^*/N_p = T_1/(q\tau_p)$, where N^* is the density of the excited ions and T_1 is the corresponding lifetime. q is the number ratio of resonant NQP over decaying excitations. This factor is diminished when the electronic excitation population is spread over several levels. However, q may also be increased by several processes the most prominent one being the bottleneck effect, when NQP resonant with the electronic transition are accumulated. In such a case a single electronic decay may lead to several resonant NQP. Using the data for Pr^{3+} site I, N^* is estimated from the considerations in the previous section by setting $N^* = \langle w \rangle p / r_0^3$, so that with $p = 1.25 \times 10^{-5}$ and $\langle w \rangle = 1.6 \times 10^{-4}$ we obtain $N^* \simeq 1.4 \times 10^{14}$ cm^{-3}. Setting $q = 0.1$ and using the phonon lifetime of $\tau_p \simeq 0.5$ μs we calculate $N_p = 4 \times 10^{10}$ cm^{-3} and $\Gamma_{\mathrm{NQP}} \simeq 700$ Hz. Because there are several competing phonon-relaxation processes, bottlenecking, detuning, and anharmonic relaxation, and because the quantities used in this calculation are rough estimates, the calculated broadening is somewhat arbitrary. Nevertheless, a substantial contribution to the broadening by NQP for Pr^{3+} site I is feasible. Such a contribution would lift the discrepancy between the prediction based on EFS and the observed broadening for Pr^{3+} site I.

From the level scheme in Fig. 12 and from the ν_p^{-5} law of the phonon lifetimes it is clear that the broadening by NQP is much less likely to occur for Pr^{3+} site II and for Eu^{3+} site I. This is supported by the fact that no power-dependent broadening was observed for Pr^{3+} site II and that the Eu^{3+} data could be fitted assuming EFS only.

So far we only discussed whether broadening by NQP is feasible. Concerning the dependence on the pulse strength an expression is derived in Appendix D that up to a correction term reads

$$-\ln\left(\frac{I}{I_0}\right)_{\mathrm{NQP}} \sim \langle w_1 \rangle (1 - e^{-2\gamma t_{12}}) + \langle w_2 \rangle (1 - e^{-\gamma t_{12}}). \quad (32)$$

This expression is clearly different from the corresponding Eq. (20) for EFS. For $\gamma t_{12} \ll 1$ the broadening is

$$\Gamma_{\mathrm{NQP}} \sim 2\mathcal{T}_1 + \mathcal{T}_2, \quad (33)$$

which, similar to Eq. (22) for EFS, is regarded as a signature of the broadening by NQP.[6] NQP and EFS are generally expected to simultaneously lead to a broadening. Assuming $\gamma t_{12} \ll 1$, the combination of Eqs. (22) and (33) gives $\Gamma \sim \beta \mathcal{T}_1 + \mathcal{T}_2$, $\beta \in [0,2]$. β indicates the mixing of the two effects, so that $\beta = 0$ corresponds to pure EFS and $\beta = 2$ to pure NQP broadening, respectively. Concerning Pr^{3+} site I, as mentioned above, t_{12} had to be chosen long compared to T_1 in order to detect the pulse-energy-dependent attenuation. At these times, $\Gamma \sim \beta \mathcal{T}_1 + \mathcal{T}_2$ is not applicable so that the discrimination between the broadening by EFS and NQP is more difficult. We emphasize that Equall *et al.* considered only EFS for the interpretation of the power-dependent broadening for Pr^{3+} in Y_2SiO_5.[29]

Making use of the above scattering model we also estimate the diffusion constant. The mean free path between scattering events is $\lambda = 1/(N\sigma_0)$, where N is the concentration of ions resonant with the NQP. Taking for the elastic scattering centers only the Pr^{3+} site I ions we calculate $N \simeq 1 \times 10^{18}$ cm^{-3} from which we obtain $\lambda \simeq 100$ nm for the mean free path and $D = \lambda^2/(6\tau_{\mathrm{scattering}}) = \lambda v_p/6 \simeq 1$ cm^2 s^{-1} for the diffusion constant. Furthermore, we calculate the diffusion distance within the phonon lifetime to be $\langle r^2 \rangle^{1/2} \simeq (2D\tau_p)^{1/2} \simeq 10$ μm. This value is somewhat too small if compared to the study of Bai and Kachru,[6] in which a dependence on the laser focus for areas larger than 0.025 mm^2 is reported, corresponding to a radius $r \simeq 100$ μm. Comparing the diffusion length with the 45-μm beam waist of the present experiments we suspect that only a fraction of the NQP diffuse out of the excitation area. However, with detuning of the NQP from resonance the scattering cross section decreases rapidly, so that the detuned phonons are more likely to escape from the excitation area.

IV. CLOSING REMARKS

We have studied the echo attenuation of Eu^{3+} and Pr^{3+} ions diluted in a Y_2SiO_5 crystal as a function of varying parameters. The discussion of the broadening by EFS and NQP has been based on statistical grounds. Since dephasing is a quantum coherence problem, quantum-mechanical and statistical aspects have been combined in this analysis.

We have derived expressions for EFS by diagonal and off-diagonal interactions as observed in 2PPE experiments for arbitrarily strong excitation pulses in the limit of large inhomogeneous bandwidths. An experiment has been proposed that allows one to distinguish between the two EFS contributions. The experimental results and the predictions strongly indicate that EFS by off-diagonal interactions are

negligible in the system considered in this work. We point out that this claim does not hold generally because the broadening depends on the properties of the photoactive species. Based on Stark experiments we have predicted the EFS broadening by diagonal interactions. The comparison of the predicted and measured broadening by EFS for Eu^{3+} and Pr^{3+} have revealed that the calculations are accurate to roughly a factor of 2. Inaccuracies arise from several experimental quantities that enter the calculations: oscillator strength, inhomogeneous width, guest-ion concentration, static dipole-moment differences, and the excitation probabilities by the laser pulses. We believe that these inaccuracies are the reason for the deviations between theory and experiment, rather than that modifications of the model are required.

We comment on the remarkable observation that a very low excitation density can give rise to EFS that can be detected by photon echoes. For $p\langle w\rangle \simeq 1\times 10^{-8}$ obtained for Eu^{3+} site I in Sec. III C, the closest distance between excited ions is typically as large as 100 nm and yet, the interactions lead to measurable effects. Accounting for the small dipole-moment differences of 10^{-2} D, this observation demonstrates the power of the photon-echo spectroscopy for the investigation of extremely small changes in the environment. We argue correspondingly that TLS even at very low concentrations may lead to a detectable dephasing. This gives support to our hypothesis that differences in the optical behavior between crystals grown under nominally identical conditions can be attributed to TLS.

Concerning the effect of nonequilibrium phonons, our predictions are only qualitative and estimates based on a phonon-scattering model remain vague. The attenuation by NQP depends crucially on the energy-level scheme of the ions because the broadening is dominated by the resonance between the NQP and transitions of the ions. The investigation of 2PPE in other systems and especially of the NQP properties is required to shed more light on this type of broadening. The characteristics of the broadening by EFS and NQP as a function of the pulse intensities facilitate the distinction between the two broadening processes. For sufficiently small pulse energies, the representation of the broadening as a function of $\beta\mathcal{T}_1+\mathcal{T}_2$, as proposed in this paper, provides a means to graphically get information about the two broadening mechanisms. The quality of the present experimental results has turned out to be not good enough to unambiguously attribute part of the broadening to NQP for Pr^{3+} site I in Y_2SiO_5. From the estimates, however, a considerable NQP broadening is plausible. We argue that due to the 23-cm^{-1} level spacing in the excited state of Pr^{3+} in LaF_3 (Ref. 7) NQP could also be of importance in a standard 2PPE experiment where the pulse-energy dependence of the linewidth was solely attributed to EFS.[34]

We have further studied the dependence of the echo attenuation as a function of the frequency position in the inhomogeneously broadened band for Eu^{3+} in Y_2SiO_5. The results confirm the prediction that the echo attenuation by diagonal EFS depends linearly on the excitation density in the system. However, we have shown that such a dependence also holds for the attenuation by off-diagonal EFS as well as by NQP, so that these experiments do not allow for the distinction between the tree-broadening processes.

The experiments in this work were carried out for an optically thin crystal and also the theoretical considerations have been based on the thin-crystal approximation. The situation may dramatically change for optically thick crystals, because the effect of light propagation cannot be disregarded anymore. Longitudinal inhomogeneities in the laser field may significantly change the characteristics of echo dependence on t_{12} and on the pulse intensities.

Summarizing, we have studied the broadening induced by various dynamical processes. We have compared the predictions with the experimental results obtained from a single system and reasonable agreement has been achieved. The consideration of the characteristic behavior and of the quantitative estimates may render possible the selection of systems specially suited for the investigation of a particular broadening mechanism in further studies.

ACKNOWLEDGMENTS

We would like to thank Dr. Masaharu Mitsunaga for the extensive loan of a crystal and for helpful discussions. We are grateful to Professor J. Skinner for private communications and we acknowledge stimulating discussions with Dr. G. Harms, Dr. T. Plakhotnik, and E. Donley. This work was supported by the ''Board of the Swiss Federal Institutes of Technology'' and ETH-Zürich.

APPENDIX A: RABI SOLUTION OF THE EXCITATION DENSITY

In this appendix we determine the excitation density for an inhomogeneously broadened band using the density-matrix approach. Similar calculations were considered by Zhang and Mossberg.[34] For this calculation we disregard damping for times shorter than the pulse times $\tau_{1,2}$ and consider only the w element of the Bloch vector (u,v,w) which after the first pulse is[61]

$$w(\tau_1;\Delta,\chi_1)=\frac{\Delta^2+\chi_1^2\cos(\tau_1\sqrt{\Delta^2+\chi_1^2})}{\Delta^2+\chi_1^2}w_0, \qquad \text{(A1)}$$

where Δ is the difference between the transition and the laser frequency. χ_k denotes the Rabi frequency of pulse k. We assume the initial state $(u_0,v_0,w_0)=(0,0,-1)$ and denote by w_1 the density-matrix element $\rho_{22}(\tau_1)$, so that

$$\begin{aligned} w_1=\rho_{22}(\tau_1)&=\tfrac{1}{2}[1+w(\tau_1;\Delta,\chi_1)]\\ &=\frac{\chi_1^2[1-\cos(\tau_1\sqrt{\Delta^2+\chi_1^2})]}{2(\Delta^2+\chi_1^2)}. \end{aligned} \qquad \text{(A2)}$$

The average excitation density is obtained from the integration over the inhomogeneously broadened band. Assuming that the band is of Gaussian shape, that the laser frequency is tuned to the center of the band, and that the width of the band is much larger than the Rabi frequency we approximate the spectral density by a constant equal to the density at the band center $1/(\sqrt{2\pi}\sigma_\nu)$ where σ_ν is the standard deviation of the band in units of Hz. We obtain

$$\langle w_1\rangle = \frac{\vartheta_1}{(2\pi)^{3/2}\sigma_\nu\tau_1}\int_0^\infty \frac{1-\cos(\vartheta_1\sqrt{1+x^2})}{1+x^2}dx, \quad \text{(A3)}$$

where $\vartheta_k=\chi_k\tau_k$ denotes the area of pulse k. The average excitation density depends on ϑ_1 and parametrically on the dimensionless quantity $\sigma_\nu\tau_1$. Making use of the derivation of Kunitomo and Kaburagi,[62] Eq. (A3) can be cast into

$$\langle w_1\rangle = \frac{\vartheta_1}{4\sqrt{2\pi}\sigma_\nu\tau_1}\int_0^{\vartheta_1} J_0(x)dx, \quad \text{(A4)}$$

which is easily integrated numerically by standard routines. For small ϑ_1 values, to lowest order one has

$$\langle w_1\rangle \simeq c\mathcal{T}_1, \quad c=\frac{1}{4\sqrt{2\pi}\sigma_\nu}, \quad \text{(A5)}$$

where $\mathcal{T}_k$ denotes the pulse energy, $\mathcal{T}_k=\chi_k^2\tau_k$.

The behavior of $\langle w\rangle$ as a function of ϑ is demonstrated in Fig. 9 where for clarity the index k of the pulse is omitted. For a constant $\sigma_\nu\tau$, $\langle w\rangle$ follows a universal behavior. For $\vartheta\ll\pi/2$, $\langle w\rangle$ depends quadratically on ϑ. The first maximum is found at $\vartheta^2\simeq 11.5$. For larger ϑ values the overall behavior is linear in ϑ with an oscillatory behavior superimposed. This oscillatory behavior is expected to be smoothed out in the experimental observations because of laser field inhomogeneities. On the scale of the figure the shape of the function suggests a saturation behavior. Therefore given is also the exponential behavior $0.4[1-\exp(-2.5c\,\vartheta^2)]$. A similar exponential behavior is used in Fig. 10 as a guide to the eye.

For the excitation density at time t_3 after the second pulse the Rabi solution is[61]

$$w(t_3)\simeq -\frac{[\Delta^2+\chi_1^2\cos(\tau_1\sqrt{\Delta^2+\chi_1^2})][\Delta^2+\chi_2^2\cos(\tau_2\sqrt{\Delta^2+\chi_2^2})]}{(\Delta^2+\chi_1^2)(\Delta^2+\chi_2^2)}, \quad \text{(A6)}$$

where terms depending on $\sin(\Delta t_{12})$ and $\cos(\Delta t_{12})$ are disregarded because they contribute negligibly when integrating over the offset Δ provided that $t_{12}\gg\tau_{1,2}$. Denoting by w_2 the excitation probability for an independent second pulse, we may write

$$\rho_{22}(t_3)=\tfrac{1}{2}[1+w(t_3)]=w_1+w_2-2w_1w_2. \quad \text{(A7)}$$

This result indicates that w_2 is the probability of changing state upon the second pulse because from probabilistic considerations one has $\rho_{22}(t_3)=w_1(1-w_2)+(1-w_1)w_2$ which corresponds to the right-hand side (rhs) of Eq. (A7). We point out that $\langle w_1w_2\rangle\neq\langle w_1\rangle\langle w_2\rangle$.

APPENDIX B: AVERAGE DEPHASING TIME $\langle|\theta|\rangle$

In this appendix we evaluate the expression

$$\langle|\theta|\rangle=\left\langle\left|\int_0^{t_{12}}u(t)dt-\int_{t_{12}}^{2t_{12}}u(t)dt\right|\right\rangle, \quad \text{(B1)}$$

where the average is taken over the temporal realizations of $u(t)$ and over the excitation probability dependent on the offset Δ of the transition frequency relative to the laser frequency. The notation follows the one used in the main text. As outlined there, $u(t)$ changes states stochastically because of the two excitation pulses with probabilities w_1 and w_2 and because of the spontaneous emission according to the decay rate γ. The average over the offset and the temporal realization can be taken independently. We find

$$\langle|\theta|\rangle=\langle w_1(1-w_2)\rangle F_1+\langle(1-w_1)w_2\rangle F_2+\langle w_1w_2\rangle F_3, \quad \text{(B2)}$$

where the first term on the rhs arises when the ion under consideration is excited by the first pulse and does not change state as a result of the second pulse. The second term denotes the contribution of an ion that was not excited by the first pulse, but, however, is excited by the second pulse. The third term accounts for possible changes of state by both pulses. The prefactors are conditional probabilities of occurrence with the averages taken over the offset frequency.

F_1, F_2, and F_3 are calculated from averages over particular temporal realizations of $u(t)$. For F_1 we find

$$F_1=\gamma\left[\int_0^{t_{12}}xe^{-x\gamma}dx+\int_{t_{12}}^{2t_{12}}(2t_{12}-x)e^{-x\gamma}dx\right], \quad \text{(B3)}$$

where the first and second term on the right-hand side are the contributions when the excitation decays spontaneously in the time interval $[0,t_{12}]$ and $[t_{12},2t_{12}]$, respectively. The integration is straightforward and yields

$$F_1=\gamma^{-1}(1-e^{-t_{12}\gamma})^2. \quad \text{(B4)}$$

For F_2 we have

$$F_2=\gamma\left[\int_{t_{12}}^{2t_{12}}(x-t_{12})e^{-(x-t_{12})\gamma}dx+t_{12}\int_{2t_{12}}^{\infty}e^{-(x-t_{12})\gamma}dx\right], \quad \text{(B5)}$$

where the first term arises when spontaneous decays occur in the interval $[t_{12},2t_{12}]$ and the second term when there is no such decay. Integration gives

$$F_2=\gamma^{-1}(1-e^{-t_{12}\gamma}). \quad \text{(B6)}$$

The most involved term is F_3 being

$$F_3=\gamma^2\int_0^{t_{12}}dx\int_{t_{12}}^{2t_{12}}dy|x-(y-t_{12})|e^{-[x+(y-t_{12})]\gamma}+\gamma^2\int_0^{t_{12}}dx\int_{2t_{12}}^{\infty}dy|x-t_{12}|e^{-[x+(y-t_{12})]\gamma}+\gamma t_{12}\int_{t_{12}}^{\infty}e^{-x\gamma}dx, \tag{B7}$$

where the first term arises when a spontaneous decay occurs in the intervals $[0,t_{12}]$ and $[t_{12},2t_{12}]$, the second when a spontaneous decay takes place only in the interval $[0,t_{12}]$, and the third when there is no such an event. Integration yields

$$F_3=F_2=\gamma^{-1}(1-e^{-t_{12}\gamma}). \tag{B8}$$

Inserting Eqs. (B3) and (B8) into Eq. (B2) we obtain

$$\langle|\theta|\rangle=\langle w_1(1-w_2)\rangle\gamma^{-1}(1-e^{-t_{12}\gamma})^2+\langle w_2\rangle\gamma^{-1}(1-e^{-t_{12}\gamma}). \tag{B9}$$

For the two limiting cases $\langle w_2\rangle\to 0$ and $\langle w_1\rangle\to 0$ Eq. (B9) corresponds to Eq. (22) of Ref. 32 with $t_s=0$ and $t_s=t_{12}$, respectively. For weak pulses $\langle w_1w_2\rangle$ is negligible if compared with $\langle w_1\rangle$ so that the weight factor of the first term in Eq. (B9) can be approximated by $\langle w_1\rangle$.

Making use of Eq. (11) we find that for weak pulses

$$\langle|\theta|\rangle\simeq c\gamma^{-1}\mathcal{T}_1(1-e^{-t_{12}\gamma})^2+c\gamma^{-1}\mathcal{T}_2(1-e^{-t_{12}\gamma}), \tag{B10}$$

which is considered in Eq. (21) of the main text. For $\gamma t_{12}\ll 1$, Eq. (B9) is approximated by

$$\langle|\theta|\rangle\simeq\langle w_2\rangle t_{12}\simeq c\mathcal{T}_2t_{12}, \tag{B11}$$

where the latter equality applies for a weak second pulse. This expression is used in Eq. (22) of the main text.

APPENDIX C: EFS BY OFF-DIAGONAL INTERACTIONS

In this appendix we are concerned with the analysis of the rhs of Eq. (24) of the main text that we denote by Φ:

$$\Phi=p\sum_k{}'\ (1-\langle\exp\{-i\theta_k\sigma_{jk}[\sqrt{J_{jk}^2+(\Delta_{jk}/2)^2}-|\Delta_{jk}/2|]\}\rangle_{\theta_k,\Delta_{jk}}), \tag{C1}$$

where the average is taken over the realizations of θ_k and over the distribution of Δ_{jk}. We first consider the case of scrambler excitations shifted by a fixed frequency $\Delta\omega_s$ so that $\Delta_{jk}=|\Delta\omega_s|$. In the continuum approximation Eq. (C1) writes

$$\Phi\simeq 4\pi\rho_0p\left\langle\int_0^{\infty}dr\ r^2(1-\cos\{\theta[\sqrt{J_0^2\kappa^2(\Omega)(r_0/r)^6+(\Delta\omega_s/2)^2}-|\Delta\omega_s/2|]\})\right\rangle_{\theta,\Omega}, \tag{C2}$$

where ρ_0 and p have the meaning of Sec. III C and the average is taken over θ and the angular configuration indicated by Ω. Changing variables ($r^{-3}\to x$) the integration by parts gives

$$\Phi=\frac{4\pi}{3}r_0^3\rho_0pJ_0^2\left\langle|\theta|\kappa^2(\Omega)\int_0^{\infty}\frac{\sin\{|\theta|[\sqrt{J_0^2\kappa^2(\Omega)x^2+(\Delta\omega_s/2)^2}-|\Delta\omega_s/2|]\}}{\sqrt{J_0^2\kappa^2(\Omega)x^2+(\Delta\omega_s)^2}}dx\right\rangle_{\theta,\Omega}. \tag{C3}$$

We substitute $y=\sqrt{J_0^2\kappa^2(\Omega)x^2+(\Delta\omega_s/2)^2}-|\Delta\omega_s/2|$ so that

$$\Phi=\frac{4\pi}{3}r_0^3\rho_0pJ_0\langle|\kappa|\rangle\left\langle|\theta|\int_0^{\infty}dy\frac{1}{\sqrt{y(y+|\Delta\omega_s|)}}\sin(|\theta|y)\right\rangle_{\theta}. \tag{C4}$$

Integration gives[63]

$$\Phi=\frac{4\pi}{3}r_0^3\rho_0pJ_0\langle|\kappa|\rangle\times\langle|\theta|\mathrm{Im}\{e^{-i|\theta||\Delta\omega_s/2|}K_0(-i|\theta||\Delta\omega_s/2|)\}\rangle_{\theta} \tag{C5}$$

where $K_0(x)$ is the zeroth order Bessel function of third kind and Im denotes the imaginary part. Considering the asymptotic behavior[64]

$$\mathrm{Im}\{e^{-ix}\mathrm{K}_0(-ix)\}\simeq\begin{cases}\pi/2, & x\ll 1\\ \sqrt{\dfrac{\pi}{4x}}, & x\gg 1,\end{cases} \tag{C6}$$

we obtain

$$\Phi\simeq\begin{cases}(2\pi^2/3)r_0^3\rho_0pJ_0\langle|\kappa|\rangle\langle|\theta|\rangle, & \langle|\theta|\rangle|\Delta\omega_s|\ll 1\\ (2\pi)^{3/2}(1/3)r_0^3\rho_0pJ_0\langle\sqrt{|\theta|}\rangle/\sqrt{|\Delta\omega_s|}, & \langle|\theta|\rangle|\Delta\omega_s|\gg 1.\end{cases} \tag{C7}$$

Next we consider the case where Δ_{jk} are uniformly distributed random variables restricted to the range $[-\Delta_{\max},\Delta_{\max}]$. Thus Eq. (C2) takes the form

$$\Phi \simeq \frac{4\pi\rho_0 p}{\Delta_{\max}} \Bigg\langle \int_0^{\Delta_{\max}} d\Delta \times \int_0^{\infty} dr\ r^2 (1-\cos\{\theta[\sqrt{J_0^2\kappa^2(\Omega)(r_0/r)^6+(\Delta/2)^2} - (\Delta/2)]\}) \Bigg\rangle_{\theta,\Omega}. \tag{C8}$$

Making use of Eqs. (C3)–(C5) we have

$$\Phi = \frac{4\pi}{3\Delta_{\max}} r_0^3 \rho_0 p J_0 \langle|\kappa|\rangle \times \left\langle |\theta| \int_0^{\Delta_{\max}} d\Delta\ \mathrm{Im}\{e^{-i|\theta|\Delta/2} K_0(-i|\theta|\Delta/2)\} \right\rangle_{\theta}. \tag{C9}$$

By numerical inspection we have noticed that the Padé-type approximation

$$\mathrm{Im}\{e^{-ix}K_0(-ix)\} \simeq \frac{\pi}{2\sqrt{1+\pi x}}, \tag{C10}$$

reproduces the exact result very reasonably for $x \in [0,\infty]$ with a maximum relative deviation of less than 4%. By substituting Eq. (C10) into Eq. (C9) we obtain

$$\Phi \simeq \frac{2\pi^2}{3\Delta_{\max}} r_0^3 \rho_0 p J_0 \langle|\kappa|\rangle \left\langle |\theta| \int_0^{\Delta_{\max}} \frac{d\Delta}{\sqrt{1+\pi\Delta|\theta|/2}} \right\rangle_{\theta}$$

$$= \frac{8\pi}{3\Delta_{\max}} r_0^3 \rho_0 p J_0 \langle|\kappa|\rangle (\langle\sqrt{1+\pi\Delta_{\max}|\theta|/2}\rangle_{\theta} - 1). \tag{C11}$$

Taking into account that θ is not broadly distributed, we approximate expression (C11) by the limiting cases

$$\Phi \simeq \begin{cases} (2\pi^2/3) r_0^3 \rho_0 p J_0 \langle|\kappa|\rangle\langle|\theta|\rangle, & \langle|\theta|\rangle\Delta_{\max} \ll 1 \\ (2\pi)^{3/2}(1/3) r_0^3 \rho_0 p J_0 \langle\sqrt{|\theta|}\rangle/\sqrt{\Delta_{\max}}, & \langle|\theta|\rangle\Delta_{\max} \gg 1, \end{cases} \tag{C12}$$

which are considered in Eq. (26) of the main text.

APPENDIX D: NUMBER OF SPONTANEOUS DECAY EVENTS

In this appendix we consider the number $\langle N\rangle$ of spontaneous decays of electronic excitations in the time $2t_{12}$. These decays may generate nonequilibrium phonons. We follow the scheme of Appendix B and describe $\langle N\rangle$ in terms of the excitation probability w_1 by the first pulse and by the probability w_2 of changing state upon the second pulse and of the decay rate γ.

The probability for one spontaneous decay can be given as the sum of three terms:

$$P_1 = \langle w_1(1-w_2)\rangle(1-e^{-2\gamma t_{12}}) + \langle(1-w_1)w_2\rangle(1-e^{-\gamma t_{12}}) + \langle w_1 w_2\rangle(1-e^{-\gamma t_{12}})e^{-\gamma t_{12}}, \tag{D1}$$

where the first term denotes the probability that an excitation is induced by the first pulse, that the state is not altered by the second pulse, and a spontaneous decay occurs in the period between the first pulse and the echo. The second term is the probability that an excitation is induced only by the second pulse followed by a decay in the period between the second pulse and the echo. The third term denotes the probability that an excitation is induced by the first pulse and that a spontaneous decay occurs in the interpulse period followed again by an excitation without further decay. Analogously, for the probability of two decay events we write

$$P_2 = \langle w_1 w_2\rangle(1-e^{-\gamma t_{12}})^2, \tag{D2}$$

which is the probability that excitations are induced by the first and second pulse and decays occur in the interpulse period and in the period between the second pulse and the echo. The expectation value of the number of decay events thus is

$$\langle N\rangle = P_1 + 2P_2 = \langle w_1\rangle(1-e^{-2\gamma t_{12}}) + \langle w_2(1-w_1)\rangle(1-e^{-\gamma t_{12}}) - 2\langle w_1 w_2\rangle(1-e^{-\gamma t_{12}})e^{-\gamma t_{12}}. \tag{D3}$$

For either $\langle w_1\rangle = 0$ or $\langle w_2\rangle = 0$ we recover the two trivial cases where either only the first or the second pulse induces an excitation. For small $\langle w_1\rangle$ and $\langle w_2\rangle$ values Eq. (D3) reduces to

$$\langle N\rangle \simeq \langle w_1\rangle(1-e^{-2\gamma t_{12}}) + \langle w_2\rangle(1-e^{-\gamma t_{12}}), \tag{D4}$$

which was considered in Eq. (32) of the main text. For $\gamma t_{12} \ll 1$, Eq. (D3) can be approximated by

$$\langle N\rangle \simeq [(1-e^{-2c\mathcal{T}_1}) + \tfrac{1}{2}(1-e^{-2c\mathcal{T}_2})]\gamma t_{12}. \tag{D5}$$

Finally for weak pulses and for $\gamma t_{12} \ll 1$ we find

$$\langle N\rangle \simeq (2\mathcal{T}_1 + \mathcal{T}_2) c\gamma t_{12}, \tag{D6}$$

which is considered in Eq. (33) of the main text.

*Author to whom correspondence should be sent. Electronic address: fgraf@phys.chem.ethz.ch

[1] J. Becquerel, Phys. Z. **8**, 632 (1908).

[2] R.M. Macfarlane and R. Shelby, in *Spectroscopy of Solids Containing Rare-Earth Ions*, edited by A. Kaplyanskii and R. Macfarlane (Elsevier Science, North-Holland, Amsterdam, 1987), Chap. 3, and references therein.

[3] T.W. Mossberg, Opt. Lett. **7**, 77 (1982); M. Mitsunaga, R. Yano, and N. Uesugi, *ibid.* **16**, 1890 (1991); R. Yano, M. Mitsunaga, and N. Uesugi, J. Opt. Soc. Am. B **9**, 992 (1992); S. Köll and U. Elman, Opt. Lett. **18**, 1834 (1993); H. Lin, T. Wang, G. Wilson, and T.W. Mossberg, *ibid.* **20**, 91 (1995); F.R. Graf, B.H. Plagemann, E.S. Maniloff, S.B. Altner, A. Renn, and U.P. Wild, *ibid.* **21**, 284 (1996); X.A. Shen, A. Nguyen, J. Perry, D. Huestis, and R. Kachru, Science **278**, 96 (1997).

[4] R.M. Macfarlane and R.M. Shelby, Opt. Commun. **39**, 169 (1981).

[5] J. Huang, J.M. Zhang, A. Lezama, and T.W. Mossberg, Phys. Rev. Lett. **63**, 78 (1989).

[6] Y.S. Bigs and R. Kachru, Phys. Rev. B **46**, 13 735 (1992).

[7] R.M. Macfarlane and R.S. Meltzer, J. Phys. (Paris) Colloq. **46**, C7-253 (1985).
[8] R.L. Cone and G.K. Liu, Bull. Am. Phys. Soc. **33**, 676 (1988); G.K. Liu and R.L. Cone, Phys. Rev. B **41**, 6193 (1990).
[9] Y.S. Bai and M.D. Fayer, Chem. Phys. **128**, 135 (1988).
[10] M. Mitsunaga, T. Takagahara, R. Yano, and N. Uesugi, Phys. Rev. Lett. **68**, 3216 (1992).
[11] S. Altner, M. Mitsunaga, G. Zumofen, and U.P. Wild, Phys. Rev. Lett. **76**, 1747 (1996).
[12] S. Mukamel, *Principles of Nonlinear Optical Spectroscopy* (Oxford University Press, New York, 1995).
[13] E. Geva and J.L. Skinner, J. Chem. Phys. **107**, 7630 (1997).
[14] R.W. Equall, Y. Sun, R.L. Cone, and R.M. Macfarlane, Phys. Rev. Lett. **72**, 2179 (1994).
[15] J. Klauder and P. Anderson, Phys. Rev. **125**, 912 (1962).
[16] A. Abragam and B. Bleaney, *Electron Paramagnetic Resonance of Transition Ions* (Dover Press, New York, 1986).
[17] D.E. MacCumber and M.D. Struge, J. Appl. Phys. **34**, 1682 (1963); W.R. Babbitt, A. Lezama, and T.W. Mossberg, Phys. Rev. B **39**, 1987 (1989).
[18] G.P. Flinn, K.W. Jang, M.L. Jones, R.S. Meltzer, and R.M. Macfarlane, Phys. Rev. B **49**, 5821 (1994).
[19] P.W. Anderson, B.L. Halperin, and C.M. Varma, Philos. Mag. **25**, 1 (1971).
[20] A. Suarez and R. Silbey, Chem. Phys. Lett. **218**, 445 (1994).
[21] P.W. Anderson and P.R. Weiss, Rev. Mod. Phys. **15**, 269 (1953).
[22] R. Kubo, in *Fluctuation, Relaxation and Resonance in Magnetic Systems*, edited by D. ter Haar (Oliver and Boyd Ltd., Edinburgh, 1962).
[23] W.B. Mims, Phys. Rev. **168**, 370 (1968); W. B. Mims, in *Electron Paramagnetic Resonance*, edited by S. Gschwind (Plenum, New York, 1972), Chap. 4, p. 263.
[24] D.R. Taylor and J. Hessler, Phys. Lett. **50A**, 205 (1974).
[25] P. Hu and S.R. Hartmann, Phys. Rev. B **9**, 1 (1974).
[26] P. Hu and L.R. Walker, Phys. Rev. B **18**, 1300 (1978).
[27] R.M. Shelby and R.M. Macfarlane, Opt. Commun. **27**, 399 (1978).
[28] R.G. DeVoe, A. Wokaun, S.C. Rand, and R.G. Brewer, Phys. Rev. B **23**, 3125 (1981).
[29] R.W. Equall, R.L. Cone, and R.M. Macfarlane, Phys. Rev. B **52**, 3963 (1995).
[30] J. Ganem, Y.P. Wang, R.S. Meltzer, W.M. Yen, and R.M. Macfarlane, Phys. Rev. Lett. **66**, 695 (1991); R.M. Macfarlane, R. Wannemacher, D. Boye, Y. P. Wang, and R. S. Meltzer, J. Lumin. **48**, 313 (1991); A. Szabo, T. Muramoto, and R. Kaarli, Phys. Rev. B **42**, 7769 (1990).
[31] P.F. Liao and S.R. Hartmann, Opt. Commun. **8**, 310 (1973).
[32] S. Altner, G. Zumofen, U.P. Wild, and M. Mitsunaga, Phys. Rev. B **54**, 17 493 (1996).
[33] J. Huang, J. Zhang, and T. Mossberg, Opt. Commun. **75**, 29 (1990).
[34] J. Zhang and T.W. Mossberg, Phys. Rev. B **48**, 7668 (1993).
[35] L. Root and J.L. Skinner, J. Phys. Chem. **81**, 5310 (1984).
[36] L. Root and J.L. Skinner, Phys. Rev. B **32**, 4111 (1985).
[37] Y.Y. Asadullin, Laser Phys. **2**, 965 (1992).
[38] W. Warren and A. Zewail, J. Phys. Chem. **85**, 2309 (1981); J. Chem. Phys. **78**, 2298 (1983).
[39] J. Skinner, H. Andersen, and M. Fayer, J. Chem. Phys. **75**, 3195 (1981).
[40] S. Altner, U.P. Wild, and M. Mitsunaga, Chem. Phys. Lett. **237**, 406 (1995).
[41] *Nonequilibrium Phonon Dynamics*, Vol. 14 of *NATO Advanced Study Institute, Series B: Physics*, edited by W. Bron (Plenum Press, New York, 1984).
[42] S. Kröll, E.Y. Xu, M.K. Kim, R. Kachru, and M. Mitsunaga, Phys. Rev. B **41**, 11 568 (1990); S. Kröll, E.Y. Xu, and R. Kachru, *ibid.* **44**, 30 (1991).
[43] Baozhu Luo and S. Kröll, Phys. Rev. B **54**, 9834 (1996).
[44] K. Holliday, M. Croci, E. Vauthey, and U.P. Wild, Phys. Rev. B **47**, 14 741 (1993).
[45] B.A. Maksimov, Y.A. Kharitonov, V.V. Illyukin, and N.B. Belov, Dokl. Akad. Nauk SSSR **183**, 1072 (1968) [Sov. Phys. Dokl. **13**, 1188 (1969)].
[46] R. Yano, M. Mitsunaga, and N. Uesugi, Opt. Lett. **16**, 1884 (1991).
[47] A. Davydov, *Theory of Molecular Excitons* (Plenum Press, New York, 1971).
[48] A. Blumen, J. Klafter, and G. Zumofen, in *Optical Spectroscopy of Glasses*, edited by I. Zschokke (Reidel, Dordrecht, 1986), p. 199.
[49] G. Mahan, Phys. Rev. **153**, 983 (1967).
[50] S.R. Polo and M.K. Wilson, J. Chem. Phys. **23**, 2376 (1955).
[51] A.P. Kulesski, A.M. Korovkin, A.V. Kruzkalov, L.V. Viktorov, and B.V. Shugin, J. Appl. Spectrosc. **48**, 446 (1988).
[52] F.R. Graf, A. Renn, U.P. Wild, and M. Mitsunaga, Phys. Rev. B **55**, 11 225 (1997).
[53] F.R. Graf, Ph.D. thesis, ETH-Zürich, 1998.
[54] C.F. Boettcher, *Theory of Electric Polarization*, 2nd ed. (Elsevier, Amsterdam, 1973), Vol. 1.
[55] G.K. Liu, R.L. Cone, M.F. Joubert, B. Jacquier, and J.L. Skinner, J. Lumin. **45**, 387 (1990).
[56] R. Baumgartner, M. Engelhardt, and K.F. Renk, Phys. Rev. Lett. **47**, 1403 (1981).
[57] R. Orbach and L. Vredevoe, Physics (Long Island City, NY) **1**, 91 (1964).
[58] K.F. Renk, in *Detection of High-Frequency Phonons by Phonon-induced Fluorescence*, edited by W. Eisenmenger and A. Kaplyanski (Elsevier, Amsterdam, 1986), Vol. 16, Chap. 6, pp. 277–372.
[59] X.A. Shen and R. Kachru, J. Opt. Soc. Am. B **11**, 591 (1994).
[60] W. Demtröder, *Laser Spectroscopy, Basic Concepts and Instrumentation* (Springer, Berlin, 1996).
[61] L. Allen and J.H. Eberly, *Optical Resonance and Two-Level Atoms* (Wiley, New York, 1975).
[62] M. Kunitomo and M. Kaburagi, Phys. Rev. A **29**, 207 (1983).
[63] I. Gradshteyn and I. Ryzhik, *Tables of Integrals, Series, and Products* (Academic Press, New York, 1980).
[64] M. Abramowitz and A. Stegun, *Handbook of Mathematical Functions* (Dover Publications, New York, 1972).